Data-efficient Large Scale Place Recognition with Graded Similarity Supervision

María Leyva-Vallina University of Groningen

University of Twente

Nicolai Petkov University of Groningen

m.leyva.vallina@rug.nl

n.strisciuglio@utwente.nl

Nicola Strisciuglio

n.petkov@rug.nl

Abstract

Visual place recognition (VPR) is a fundamental task of computer vision for visual localization. Existing methods are trained using image pairs that either depict the same place or not. Such a binary indication does not consider continuous relations of similarity between images of the same place taken from different positions, determined by the continuous nature of camera pose. The binary similarity induces a noisy supervision signal into the training of VPR methods, which stall in local minima and require expensive hard mining algorithms to guarantee convergence. Motivated by the fact that two images of the same place only partially share visual cues due to camera pose differences, we deploy an automatic re-annotation strategy to re-label VPR datasets. We compute graded similarity labels for image pairs based on available localization metadata. Furthermore, we propose a new Generalized Contrastive Loss (GCL) that uses graded similarity labels for training contrastive networks. We demonstrate that the use of the new labels and GCL allow to dispense from hard-pair mining, and to train image descriptors that perform better in VPR by nearest neighbor search, obtaining superior or comparable results than methods that require expensive hard-pair mining and re-ranking techniques.

1. Introduction

Visual place recognition (VPR) is an important task of computer vision, and a fundamental building block of navigation systems for autonomous vehicles [23, 51]. It is approached either with structure-based methods, namely Structure-from-Motion [36] and SLAM [25], or with image retrieval [2, 14, 19, 29, 30, 49]. The former focus on precise relative camera pose estimation [34, 35]. The latter aim at learning image descriptors for effective retrieval of similar images to a given query in a nearest search approach [28]. The goal of descriptor learning is to ensure images of the same place to be projected onto close-by points in a latent space, and images of different places to be projected onto distant points [8,9,20]. Contrastive [18,30] and triplet [2,21,22,27] loss were used for this goal and resulted







(a) reference image

(b) GPS distance 6m positive

(c) GPS distance 25.6m negative

Figure 1. (a) A place in the city of Amman. (b) An image taken 6m away is labeled as positive (same place), while (c) an image taken 25.6m away is labeled as negative (not the same place) despite sharing a lot of visual cues.

in state-of-the-art performance on several VPR benchmarks.

VPR methods are normally trained using image pairs labelled to indicate they either depict the same place or not, in a binary fashion. In practice, images of a certain place can be taken from different positions, i.e. with a different camera pose, and thus share only a part of their visual cues (or surface in 3D). In existing datasets, two images are usually labeled to be of the same place (positive) if they are taken within a predefined range (usually 25m) computed using e.g. GPS metadata. This creates ambiguous cases. For instance, Figure 1 shows a reference image (a) of a place and two other pictures taken 6m (b) and 25.6m (c) away from its position. The images are respectively labeled as positive and negative match, although they share many visual cues (e.g. the building on the right). Binary labels are thus noisy and interfere with the training of VPR networks, that usually stall in local minima. To address this, resource- and timecostly hard pair mining strategies are used to compose the training batches. For example, training NetVLAD [2] on the Mapillary Street Level Sequences (MSLS) dataset [48] can take more than 20 days on an Nvidia v100 gpu due to the complexity of pair mining. We instead build on the observation that two images depict the same place only to a certain degree of shared cues, namely a degree of similarity, and propose to embed this information in new continuous labels for existing datasets that can be used to reduce the effect of noise in the training of effective VPR methods.

In this paper we exploit camera pose metadata or 3D information associated to image pairs as a proxy to estimate an

approximate degree of similarity (hereinafter, graded similarity) between images of the same place, and use it to relabel popular VPR datasets. Graded similarity labels can be used to pick easy- and hard-pairs and compose training batches without complex pair-mining, thus speeding-up the training of VPR networks and enabling an efficient use of data. Furthermore, we embed the graded similarity into a Generalized Contrastive Loss (GCL) function that we use to train a VPR pipeline. The intuition behind this choice is that the update of network weights should not be equal for all training pairs, but rather be influenced by their similarity. The representations of image pairs with larger graded similarity should be pushed together in the latent space more strongly than those of images with a lower graded similarity. The distance in the latent space is thus expected to be a better measure of ranking images according to their similarity, avoiding the use of expensive re-ranking to improve retrieval results. We validate the proposed approaches on several VPR benchmark datasets. To the best of our knowledge, this work is the first to use graded similarity for large-scale place recognition, and paying attention to data-efficient training.

We summarize the contributions of this work as:

- new labels for VPR datasets indicating the graded similarity of image pairs. We computed the labels with automatic methods that use camera pose metadata included with the images or 3D surface information;
- a generalized contrastive loss (GCL) that exploits graded similarity of image pairs to learn effective descriptors for VPR;
- an efficient VPR pipeline trained without hard-pair mining, and that does not require re-ranking. Training our pipeline with a VGG-16 backbone converges $\sim 100x$ faster than NetVLAD with the same backbone, achieving higher VPR results on several benchmarks. The efficiency of our scheme enables training larger backbones in a short time.

2. Related works

Place recognition as image retrieval. Visual place recognition is widely addressed as a metric learning problem, in which the descriptors of images of a place are learned to be close together in a latent space [9]. Existing methods optimize ranking loss functions, such as contrastive, triplet or average precision [12, 30, 31]. NetVLAD [2] is milestone of VPR and builds on a triplet network with an endto-end trainable VLAD layer. It requires a computationally-and memory-expensive hard-pair mining to compose proper batches and guarantee convergence. SARE [21] uses a NetVLAD backbone trained with a probabilistic attractive and repulsive mechanism, also making use of hard-pair mining. Hard-pair mining addresses issues of the training

stalling in local minima due to noisy binary labels, and is used to compose the training batches so that hard pairs are selected for the training [2]. We instead use image metadata (e.g. camera pose as GPS and compass) to a-priori estimate the graded similarity of image pairs, and subsequently use it to balance hard- and easy-pairs in the training batches. This allows to train VPR models using the graded similarity of images and avoiding hard-pair mining.

Training with noisy binary labels produces image descriptors with drawbacks in nearest neighbor search retrieval, and re-ranking algorithms are necessary to post-process the retrieved results and increase VPR performance [6, 32]. Patch-NetVLAD [14] builds on a NetVLAD backbone and performs multi-scale aggregation of NetVLAD descriptors to re-rank retrieval results. A transformer architecture named TransVPR was trained using a triplet loss function and hard-pair mining in [46]. The retrieval step is combined with a costly re-ranking strategy to improve the retrieval results. We instead focus on using more informative and robust image pair labels to avoid noisy training and obtain more effective image descriptors for nearest neighbor search, with no necessity of performing re-ranking.

Image graded similarity. Soft assignment to positive and negative classes of image pairs was investigated in [42], where weighting of the assignment was based on the Euclidean distance between the GPS coordinates associated to the images. As the GPS distance induced label noise in the training process, hard-negative pair mining was still necessary to train VPR networks. In [11], image region similarity was coupled with the GPS weak labels in a self-supervised framework to mine hard positive samples. In [5], the authors formulated the VPR metric learning as a classification problem, splitting image training into classes based on similar GPS locations to facilitate large-scale city-wide recognition. Camera pose was used in [4] to estimate the camera frustum overlap and regress descriptors for camera (re-)localization in small-scale (indoor) environments. In [16], a weighting scheme for the contrastive loss function is proposed as a function of the distance in the latent space, which requires an extra step of normalization of the distances to avoid a divergent training. In this work, we relabel VPR datasets using camera pose and field of view overlap, or ratio of shared 3D surface as proxies to estimate the graded similarity of training image pairs. We compute the new labels once, and use them to select the training batches and directly in the optimization of the networks to obtain effective descriptors for VPR in a data-efficient manner.

Relation and difference with prior works. We undertake a different direction than previous works, and propose a simplified way to learn image descriptors for retrieval-based VPR. We use contrastive architectures without hard-pair mining and exploit the graded similarity of image pairs to learn robust descriptors. Instead of developing algorithmic solu-

tions (e.g. hard-pair mining or re-ranking) to achieve better VPR results by increasing the complexity of the methods, we focus on data-efficiency and improve similarity labels to better exploit the training data. This allows to purposely keep the complexity of the architecture simpler (a convolutional backbone and a straightforward pooling strategy) than other methods. We apply prior knowledge and use metadata about the position and orientation of the cameras to estimate a more robust ground truth image similarity that enables to drop expensive hard-mining procedures and train (bigger) networks efficiently. We show that this approach leads to reduced training time and very robust descriptors that perform well in nearest neighbour search with no need of re-ranking.

3. Generalized Contrastive Learning

Preliminaries. Contrastive approaches for metric learning in visual place recognition consider training a (convolutional) neural network $\hat{f}(x)$ so that the distance of the vector representation of similar (or dissimilar) images in a latent space is minimized (or maximized). In this work, we consider siamese networks optimized using a Contrastive Loss function [13].

Let x_i and x_j be two input images, with $\hat{f}(x_i)$ and $\hat{f}(x_j)$ their descriptors. The distance of the descriptors in the latent space is the L_2 -distance $d(x_i, x_j) = \left\|\hat{f}(x_i) - \hat{f}(x_j)\right\|_2$. The Contrastive Loss \mathcal{L}_{CL} used to train the networks is defined as:

$$\mathcal{L}_{CL}(x_i, x_j) = \begin{cases} \frac{1}{2} d(x_i, x_j)^2, & \text{if } y = 1\\ \frac{1}{2} \max(\tau - d(x_i, x_j), 0)^2, & \text{if } y = 0 \end{cases}$$
(1)

where τ is the margin, an hyper-parameter that defines a boundary between similar and dissimilar pairs. The ground truth label y is binary: 1 indicates a pair of similar images, and 0 a not-similar pair of images. In practice, however, a binary ground truth for similarity may cause the trained models to provide unreliable predictions.

Generalized Contrastive Loss. We reformulate the Contrastive Loss, using a generalized definition of pair similarity as a continuous value $\psi_{i,j} \in [0,1]$. We define the Generalized Contrastive Loss function \mathcal{L}_{GCL} as:

$$\mathcal{L}_{GCL}(x_i, x_j) = \psi_{i,j} \cdot \frac{1}{2} d(x_i, x_j)^2 + (1 - \psi_{i,j}) \cdot \frac{1}{2} \max(\tau - d(x_i, x_j), 0)^2$$
 (2)

In contrast to Eq. 1, here the similarity $\psi_{i,j}$ is a continuous value ranging from 0 (completely dissimilar) to 1 (identical). By minimising the Generalized Contrastive Loss, the distance of image pairs in the latent space is optimized proportionally to the corresponding degree of similarity.

Gradient of the GCL. In the training phase, the loss function is minimized by gradient descent optimization and the weights of the network are updated by backpropagation. In the case of the Constructive Loss function, the gradient is:

$$\nabla \mathcal{L}_{CL}(x_i, x_j) = \begin{cases} d(x_i, x_j), & \text{if } y = 1\\ \min(d(x_i, x_j) - \tau, 0), & \text{if } y = 0 \end{cases}$$
(3)

The gradient is computed for all positive pairs, and corresponds to a direct minimization of their descriptor distance in the latent space. For negative pairs, the update of the network weights takes place only in the case the distance of the descriptors is within the margin τ . If the latent vectors are already at a distance higher than τ , no update is done.

The Generalized Contrastive Loss, instead, explicitly accounts for graded similarity $\psi_{i,j}$ of input pairs (x_i,x_j) to weight the learning steps, and this reflects into the gradient:

$$\nabla \mathcal{L}_{GCL}(x_i, x_j) = \begin{cases} d(x_i, x_j) + \tau(\psi_{i,j} - 1), & \text{if } d(x_i, x_j) < \tau \\ d(x_i, x_j) \cdot \psi_{i,j}, & \text{if } d(x_i, x_j) \ge \tau \end{cases}$$
(4)

The gradient of \mathcal{L}_{GCL} is modulated by the degree of similarity of the input image pairs, $\psi_{i,j}$. This results in an implicit regularization of learned latent space. In the supplementary material, we provide and compare plots of the latent space learned with the \mathcal{L}_{CL} and \mathcal{L}_{GCL} functions. At the extremes of the similarity range, for $\psi_{i,j}=0$ (completely dissimilar input images) and $\psi_{i,j}=1$ (same exact input images), the gradient is the same as in Eq. 3.

4. Experimental evaluation

4.1. Data

Mapillary Street Level Sequences. The Mapillary Street Level Sequences (MSLS) dataset is designed for life-long large-scale visual place recognition. It contains about 1.6M images taken in 30 cities across the world [48]. Images are divided into a training (22 cities, 1.4M images), validation (2 cities, 30K images) and test (6 cities, 66k images) set. The dataset presents strong challenges related to images taken at different times of the day, in different seasons and with strong variations of camera viewpoint. The images are provided with GPS data in UTM format and compass angle. According to the original paper [48], two images are considered similar if they are taken by cameras located within 25m of distance, and with less than 40° of viewpoint variation. We created (and will release) new ground truth labels for the training set of MSLS, with specification of the graded similarity of image pairs (see next Section for details). We use the MSLS dataset to train our large-scale VPR models, which we test on the validation set, and also the private test set using the available evaluation server.

OOD test data for generalization. We use out-ofdistribution (OOD) test sets, to evaluate the generalization abilities of our models and compare them with existing methods. We thus use the test and validation sets of several other benchmark datasets, namely the Pittsburgh30k [2], Tokyo24/7 [44], RobotCar Seasons v2 [24,33] and Extended CMU Seasons [3,33] datasets. In the supplementary material, we also report results on Pittsburgh250k and TokyoTM [44]. **TB-Places and 7Scenes.** We carried out experiments also using the TB-Places [18] and 7Scenes [38] datasets, which were recorded in small-scale environments. We train models on them and report the results in the supplementary material. TB-Places was recorded in an outdoor garden over two years and contains challenges related to drastic viewpoint variations, as well as illumination changes, and scenes mostly filled with repetitive texture of green color. Each image has 6DOF pose metadata. The 7Scenes dataset is recorded in seven indoor environments. It contains 6DOF pose metadata for each image and a 3D pointcloud of each scene.

The different format and type of metadata, namely 6DOF camera pose and 3D pointclouds of the scenes, are of interest to investigate different ways to estimate the ground truth graded similarity of image pairs. In the following, we present techniques to automatically re-label VPR datasets, when 6DOF pose or 3D pointclouds metadata are available.

4.2. Graded similarity labels

Images of the same place can be taken from different positions, i.e. with different camera pose, and share only part of the visual cues. On the basis of the amount of shared characteristics among images, we indeed tend to perceive images more or less similar [10]. Actual labeling of VPR datasets do not consider this and instead mark two images either similar (depicting the same place) or not (depicting different places). This does not take into account continuous relations between images, which are induced by the continuous nature of camera pose.

We combine the concept of perceived visual similarity with the continuous nature of camera pose, and design a method to automatically relabel VPR dataset by annotating the graded similarity of image pairs¹. We approximate the similarity between two images via a proxy, namely measuring the overlap of the field of view of the cameras or 3D information associated to the images.

Graded similarity for MSLS and TB-Places: field of view overlap. For MSLS and TB-Places dataset, images are provided with camera pose metadata in the form of a vector t and orientation α . The MSLS has UTM data and compass angle information associated to the images, while in TB-Places the images are provided with precise camera pose recorded with a laser tracker and IMU.

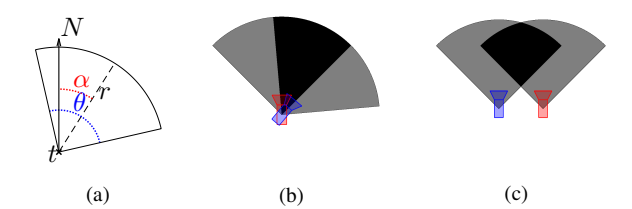


Figure 2. (a) FoV with angle θ and radius r. The point ${\bf t}$ is the camera location in the environment, and α is the camera orientation in the form of a compass angle with respect to the north N. (b) An example of FoV overal for two cameras in the same position and with orientations 40° apart. (c) An example of FoV overlap for two cameras located 25m apart but with the same orientation.

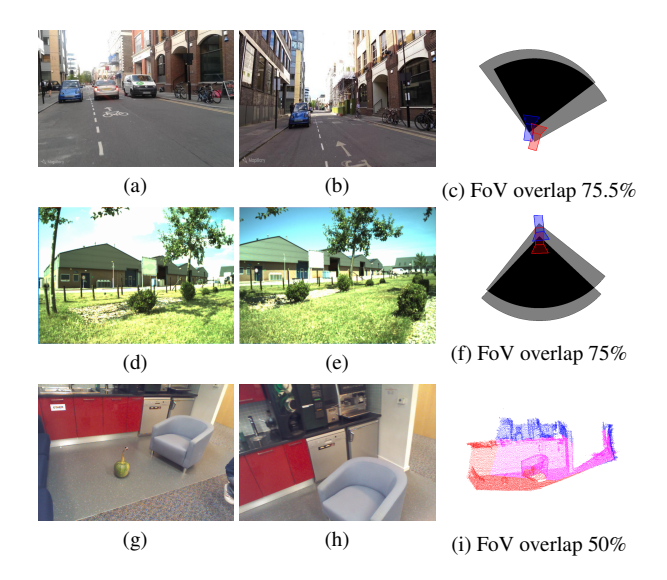


Figure 3. Examples of graded similarity estimated for MSLS (first row) and TB-Places (second row) with the FoV overlap, and 7Scenes (third row) with 3D overlap (magenta color points).

For an image, we build the field of view (FoV) of the camera as the sector of the circle centered at t with radius r, delimited by the angle range $\left[\alpha-\frac{\theta}{2},\alpha+\frac{\theta}{2}\right]$ (see Fig. 2a), where θ is the nominal size of the FoV of the camera concerned. The FoV overlap is the intersection-over-union (IoU) of the FoV of the cameras. In the first and second row of Figure 3, we show examples of the graded similarity estimated for pairs in the MSLS and TB-Places datasets. This approach differs from the camera frusta overlap [4] that needs 3D overlap measures for precise camera pose estimation.

Graded similarity for 7Scenes: 3D overlap. The 7Scenes dataset has a 3D pointcloud for each scene, and 6DOF camera pose associated to the images. In this case, we can estimate the similarity overlap differently from the cases above. We project a pair of images onto the 3D pointcloud, so that we select the points associated to the two images and measure their intersection-over-union (IoU) as a measure of the image pair similarity. A similar strategy based on

¹We release the labels at https://github.com/marialeyvallina/generalized_contrastive_loss.

maximum inliers was used for hard-pair mining in [30]. In the third row of Figure 3, we show an example of graded similarity estimation for two images in the 7Scenes dataset.

4.3. Place recognition pipeline

Embeddings. We use a fully convolutional backbone (ResNet [15], VGG16 [39] and ResNeXt [50]) with a GeM pooling layer [30], which receives as input an image $x \in R^{w_n \times h_n \times 3}$, and outputs a representation $\hat{f}(x) \in R^{d_m}$, where d_m is the number of kernels of the last convolutional layer. We train f(x) using a contrastive learning framework. **Training batch composition.** Batch composition is an important part of model training. For contrastive architectures, the selection of meaningful image tuples is crucial for the correct optimization of the model. If the selected tuples are too challenging, the training might become unstable [37]. If they are too easy, the learning might stall. This, coupled with binary pairwise labels, makes necessary to use complex descriptor-based mining strategies to ensure model convergence. The hard-negative mining strategy needed to train contrastive networks [2, 14, 21] periodically computes the descriptor of all training images and their pairwise distance to select certain pairs (tuples) of images to be used for the subsequent training steps. This is a memory- and computation-expensive procedure.

We do not perform hard-pair mining. We instead compose the training batches taking into account the graded similarity labels that we computed. We balance the pairs in the training batches on the basis of their annotated degree of similarity. For each batch, we make sure to select 50% of positive pairs (similarity higher than 50%), 25% of soft negative samples (similarity higher than 0% and lower than 50%) and 25% of hard negatives (0% similarity) – see Section 5 for results.

Image retrieval. Let us consider a set X of reference images with a known camera location, and a set Y of query images taken from unknown positions. In order to localize the camera that took the query images, similar images to the query are to be retrieved from the reference set. We compute the descriptors of the reference images $\hat{f}(x) \, \forall x \in X$, and of the query images $\hat{f}(y) \, \forall y \in Y$. For a given query descriptor $\hat{f}(y)$, image retrieval is performed by nearest neighbor search within the reference descriptors $\hat{f}(x) \, \forall x \in X$, retrieving k images ranked by the closest descriptor distance.

4.4. Performance measures

We apply widely used place recognition evaluation protocols and consider a query as correctly identified if any of the top-k retrieved images are annotated as a positive match [2, 34, 48]. We computed the following metrics. For the MSLS, Pittsburgh30k, Tokyo24/7 (Pittsburgh250k, TokyoTM, TrimBot2020 and 7Scences in the supplementary material) we compute the **Top-k recall** (**R@k**). It measures the percentage of queries for which at least a correct map image

]	MSLS	-Val	MSLS-Test						
Method	Loss	Batch	R@1	R@5	R@10	R@1	R@5	R@10				
VGG-GeM VGG-GeM		•			65.5 76.9			46.5 57.8				
VGG-GeM VGG-GeM		C					40.8 55.7	47.0 60.6				

Table 1. Effect of graded similarity labels on batch composition and model training.

is present among their k nearest neighbors retrieved. For the RobotCar Seasons v2 and the Extended CMU datasets, we compute the **percentage of correctly localized queries**. It measures the amount of images that are correctly retrieved for a given translation and rotation threshold.

5. Results and discussion

Graded similarity for batch composition and model training. We carry out a baseline experiment to evaluate the impact of the new graded similarity labels on the effectiveness of the learned descriptors. We analyze their contribution to the composition of the batches, and directly to the training of the network by using them in combination with the proposed GCL. We first consider the traditional binary labels only, and compose batches by balancing positive and negative pairs. Subsequently, we compose the batches by considering the new graded similarity labels, and select 50% of positive pairs (similarity higher than 50%), 25% of soft negative samples (similarity higher than 0% and lower than 50%) and 25% of hard negatives (0% similarity).

In Table 1, we report the results using a VGG16 backbone on the MSLS dataset. These results demonstrate that the proposed graded similarity labels are especially useful for training descriptors that perform better in nearest neighbor search retrieval, and also contribute to form better balanced batches to exploit the data in a more efficient way. In the following, all experiments use the batch composition based on graded similarity.

Comparison with existing works. We compared our results with several place recognition works. We considered methods that use global descriptors like NetVLAD [2] (with 16 and 64 clusters in the VLAD layer) and methods based on two-stages retrieval and re-ranking pipelines, such as Patch-NetVLAD [14], DELG [6] and SuperGlue [32]. We compared also against TransVPR [46], a transformer with and without a re-ranking stage. Table 2 reports the results of our method in comparison to others. All the methods included in the table are based on backbones trained on the MSLS datasets. The results of Patch-NetVLAD and TransVPR are taken from the respective papers, which also contain those of DELG and SuperGlue. When trained with VGG16 as backbone, our model (VGG16-GeM-GCL) obtains an absolute improvement of R@5 equal to 11.7% compared to

			I	MSLS.	·Val	N	ISLS-	Test		Pitts3	0k	7	Tokyoź	24/7	Robot	Car Sea	sons v2	Extend	ed CMU	Seasons
Method	PCA_w	Dim	R@1	R@5	R@10	R@1	R@5	R@10	R@1	R@5	R@10	R@1	R@5	R@10	.25m/2 $^{\circ}$.5m/5 $^{\circ}$	$5\text{m}/10^{\circ}$	$.25 \text{m/2}^{\circ}$.5m/5 $^{\circ}$	5m/10°
NetVLAD 64	N	32768	44.6	61.1	66.4	28.8	44.0	50.7	40.4	64.5	74.2	11.4	24.1	31.4	2.0	9.2	45.5	1.3	4.5	31.9
NetVLAD 64	Y	4096	70.1	80.8	84.9	45.1	58.8	63.7	68.6	84.7	88.9	34.0	47.6	57.1	4.2	18.0	68.1	3.9	12.1	58.4
NetVLAD 16	N	8192	49.5	65.0	71.8	29.3	43.5	50.4	48.7	70.6	78.9	13.0	33.0	43.8	1.8	9.2	48.4	1.7	5.5	39.1
NetVLAD 16	Y	4096	70.5	81.1	84.3	39.4	53.0	57.5	70.3	84.1	89.1	37.8	53.3	61.0	4.8	17.9	65.3	4.4	13.7	61.4
TransVPR [46]	-	-	70.8	85.1	86.9	48	67.1	73.6	73.8	88.1	91.9	-	-	-	2.9	11.4	58.6	-	-	-
SP-SuperGlue* [32]	-	-	78.1	81.9	84.3	50.6	56.9	58.3	87.2	94.8	96.4	88.2	90.2	90.2	9.5	35.4	85.4	9.5	30.7	96.7
DELG* [6]	-	-	83.2	90.0	91.1	52.2	61.9	65.4	89.9	95.4	96.7	95.9	96.8	97.1	2.2	8.4	76.8	5.7	21.1	93.6
Patch NetVLAD* [14]	Y	4096	79.5	86.2	87.7	48.1	57.6	60.5	88.7	94.5	95.9	86.0	88.6	90.5	9.6	35.3	90.9	11.8	36.2	96.2
TransVPR* [46]	-	-	86.8	91.2	92.4	63.9	74	77.5	89	94.9	96.2	-	-	-	9.8	34.7	80	-	-	-
NetVLAD-GCL	N	32768	62.7	75.0	79.1	41.0	55.3	61.7	52.5	74.1	81.7	20.3	45.4	49.5	3.3	14.1	58.2	3.0	9.7	52.3
NetVLAD-GCL	Y	4096	63.2	74.9	78.1	41.5	56.2	61.3	53.5	75.2	82.9	28.3	41.9	54.9	3.4	14.2	58.8	3.1	9.7	52.4
VGG-GeM-GCL	N	512	65.9	77.8	81.4	41.7	55.7	60.6	61.6	80.0	86.0	34.0	51.1	61.3	3.7	15.8	59.7	3.6	11.2	55.8
VGG-GeM-GCL	Y	512	72.0	83.1	85.8	47.0	60.8	65.5	73.3	85.9	89.9	47.6	61.0	69.2	5.4	21.9	69.2	5.7	17.1	66.3
ResNet50-GeM-GCL	N	2048	66.2	78.9	81.9	43.3	59.1	65.0	72.3	87.2	91.3	44.1	61.0	66.7	2.9	14.0	58.8	3.8	11.8	61.6
ResNet50-GeM-GCL	Y	1024	74.6	84.7	88.1	52.9	65.7	71.9	79.9	90.0	92.8	58.7	71.1	76.8	4.7	20.2	70.0	5.4	16.5	69.9
ResNet152-GeM-GCL	N	2048	70.3	82.0	84.9	45.7	62.3	67.9	72.6	87.9	91.6	34.0	51.8	60.6	2.9	13.1	63.5	3.6	11.3	63.1
ResNet152-GeM-GCL	Y	2048	79.5	88.1	90.1	57.9	70.7	75.7	80.7	<u>91.5</u>	93.9	<u>69.5</u>	81.0	85.1	6.0	21.6	72.5	5.3	16.1	66.4
ResNeXt-GeM-GCL	N	2048	75.5	86.1	88.5	56.0	70.8	75.1	64.0	81.2	86.6	37.8	53.6	62.9	2.7	13.4	65.2	3.5	10.5	58.8
ResNeXt-GeM-GCL	Y	1024	80.9	<u>90.7</u>	<u>92.6</u>	<u>62.3</u>	<u>76.2</u>	<u>81.1</u>	79.2	90.4	93.2	58.1	74.3	78.1	4.7	21.0	<u>74.7</u>	<u>6.1</u>	<u>18.2</u>	<u>74.9</u>

Table 2. Comparison to state-of-the-art methods on benchmark datasets. All methods are trained on the MSLS training set. Our top results are underlined, while overall best results are in bold. Methods using re-ranking are in the middle part of the table and marked with *.

NetVLAD-64. This shows that the proposed graded similarity labels and the GCL function contribute to learn more powerful descriptors for place recognition, while keeping the complexity of the training process lower as hard-pair mining is not used. The result improvement holds also when the descriptors are post-processed with PCA whitening.

The data- and memory-efficiency of our pipeline allows us to easily train more powerful backbones, such as ResNeXt, that is instead tricky to do for other methods due to memory and compute requirements. Our ResNeXt+GCL outperforms the best method on the MSLS test set, namely TransVPR without re-ranking by 8.9% and with re-ranking by 2.6% (absolute improvement of R@5). It compares favorably with re-ranking based methods such as Patch-NetVLAD, DELG and SuperGLUE improving the R@5 by 18.6%, 14.3% and 18.3%, respectively. We point out that we do not re-rank the retrieved images, and purposely keep the complexity of the steps at the strict necessary to perfom the VPR retrieval task. We attribute our high results mainly to the effectiveness of the descriptors learned with the GCL function using the new graded similarity labels.

Generalization to other datasets. In Table 2 and Table 3, we also report the results of generalization to Pittsburgh30k, Tokyo 24/7, RobotCar Seasons v2 and Extended CMU Seasons (plus Pittsburgh250k and TokyoTM in the supplementary materials). The models trained with the GCL function generalize well to unseen datasets, in many cases better than existing methods that retrieve the k-nearest neighbours based on descriptor distance only. Our models also generalize well to urban localization datasets like RobotCar Seasons V2 and Extended CMU Seasons, achieving up to 21.9% and 19% of correctly localized queries within 0.5m and 5°, respectively. The results of GCL-based networks are higher than those

obtained by NetVLAD, and especially higher than those of TransVPR (with no re-ranking) that uses a transformer as backbone. Note that we do not perform 6DOF pose estimation, but estimate the pose of a query image by inheriting that of the best retrieved match, and thus not compare with methods that perform refined pose estimation. This is inline with the experiments in [14].

Our models are outperformed only by methods that include a re-ranking strategies to refine the list of retrieved images, on the Pittsburgh30k, RobotCar Seasons v2 and Extended CMU Seasons datasets. However, these methods perform extra heavy computations (e.g. up to 6s per query in PatchNetVLAD [14]) to re-rank the list of retrieved images, not focusing on the representation capabilities of the learned descriptors themselves. Thus, we find a direct comparison with these methods not fair. On the contrary, these results demonstrate the fact the VPR descriptors learned used the proposed labels and GCL have better representation capabilities than those produced by other methods, achieving higher results in out-of-distribution experiments as well.

Ablation study: backbone and contrastive loss. We carried out ablation experiments using four backbones, namely VGG16 [39], ResNet50, ResNet152 [15], and ResNeXt101-32x8d (hereinafter ResNeXt) [50], and the GeM [30] global pooling layer, and an additional NetVLAD-GCL model. Extra ablation experiments with an average global pooling layer are included in the supplementary material. For each backbone, we train with the binary Contrastive Loss (CL) and our Generalized Contrastive Loss (GCL). We report the results in Table 3. The models trained with the GCL consistently outperform their counterpart trained with the CL, showing better generalization to other datasets. Moreover, we demonstrate that a VGG16-GeM architecture outperforms a more

				I	MSLS-	Val	M	SLS-	Test		Pitts30)k	1	Tokyo2	24/7	Robo	tCar Sea	sons v2	Extend	ed CMU	Seasons
Method	Loss 1	PCA_w	Dim	R@1	R@5	R@10	R@1	R@5	R@10	R@1	R@5	R@10	R@1	R@5	R@10	0.25m/2°	0.5m/5°	$5.0\text{m}/10^{\circ}$	0.25m/2°	0.5m/5°	$5.0\text{m}/10^{\circ}$
	CL	N	32768	38.5	56.6	64.1	24.8	39.1	46.1	24.7	48.3	61.1	7.0	18.1	24.8	0.9	5.2	31.5	1.0	1.4	11.1
N-AVI AD	GCL	N	32768	62.7	75.0	79.1	41.0	55.3	61.7	52.5	74.1	81.7	20.3	45.4	49.5	3.3	14.1	58.2	3.0	9.7	52.3
NetVLAD	CL	Y	4096	39.6	60.3	65.3	26.4	40.5	48.2	27.5	51.6	64.1	6.7	16.2	25.7	0.0	0.0	0.0	1.0	3.3	25.4
	GCL	Y	4096	63.2	74.9	78.1	41.5	56.2	61.3	53.5	75.2	82.9	28.3	41.9	54.9	3.4	14.2	58.8	3.1	9.7	52.4
	CL	N	512	47.0	60.3	65.5	27.9	40.5	46.5	51.2	71.9	79.7	24.1	39.4	47.0	3.1	13.2	55.0	2.8	8.6	44.5
VGG-GeM	GCL	N	512	65.9	77.8	81.4	41.7	55.7	60.6	61.6	80.0	86.0	34.0	51.1	61.3	3.7	15.8	59.7	3.6	11.2	55.8
VGG-GeM	CL	Y	512	61.4	75.1	78.5	36.3	49.0	54.1	64.7	81.5	86.8	36.2	54.0	57.8	4.2	18.7	62.5	4.4	13.4	56.5
	GCL	Y	512	72.0	83.1	85.8	47.0	60.8	65.5	73.3	85.9	89.9	47.6	61.0	69.2	5.4	21.9	69.2	5.7	17.1	66.3
	CL	N	2048	51.4	66.5	70.8	29.7	44.0	50.7	61.5	80.0	86.9	30.8	46.0	56.5	3.2	15.4	61.5	3.2	9.6	49.5
ResNet50-GeM	GCL	N	2048	66.2	78.9	81.9	43.3	59.1	65.0	72.3	87.2	91.3	44.1	61.0	66.7	2.9	14.0	58.8	3.8	11.8	61.6
Resnet50-GeW	CL	Y	1024	63.2	76.6	80.7	37.9	53.0	58.5	66.2	82.2	87.3	36.2	51.8	61.0	5.0	21.1	66.5	4.7	13.4	51.6
	GCL	Y	1024	74.6	84.7	88.1	52.9	65.7	71.9	79.9	90.0	92.8	58.7	71.1	76.8	4.7	20.2	70.0	5.4	16.5	69.9
	CL	N	2048	58.0	72.7	76.1	34.1	50.8	56.8	66.5	83.8	89.5	34.6	57.1	63.5	3.3	15.2	64.0	3.2	9.7	52.2
ResNet152-GeM	GCL	N	2048	70.3	82.0	84.9	45.7	62.3	67.9	72.6	87.9	91.6	34.0	51.8	60.6	2.9	13.1	63.5	3.6	11.3	63.1
Resnet132-Gelvi	CL	Y	2048	66.9	80.9	83.8	44.8	59.2	64.8	71.2	85.8	89.8	54.3	68.9	75.6	6.1	23.5	68.9	4.8	14.2	55.0
	GCL	Y	2048	79.5	88.1	90.1	57.9	70.7	75.7	80.7	91.5	93.9	69.5	81.0	85.1	6.0	21.6	72.5	5.3	16.1	66.4
	CL	N	2048	62.6	76.4	79.9	40.8	56.5	62.1	56.0	77.5	85.0	37.8	54.9	62.5	1.9	10.4	54.8	2.9	9.0	52.6
D. N.W. C.M	GCL	N	2048	75.5	86.1	88.5	56.0	70.8	75.1	64.0	81.2	86.6	37.8	53.6	62.9	2.7	13.4	65.2	3.5	10.5	58.8
ResNeXt-GeM	CL	Y	1024	74.3	87.0	89.6	49.9	63.8	69.4	70.9	85.7	90.2	50.8	67.6	74.3	3.8	17.2	68.2	4.9	14.4	61.7
	GCL	Y	1024	80.9	90.7	92.6	62.3	76.2	81.1	79.2	90.4	93.2	58.1	74.3	78.1	4.7	21.0	74.7	6.1	18.2	74.9

Table 3. Ablation study on backbone, Contrastive (CL) vs Generalized Contrastive (GCL) loss, and PCA. All models are trained on MSLS.

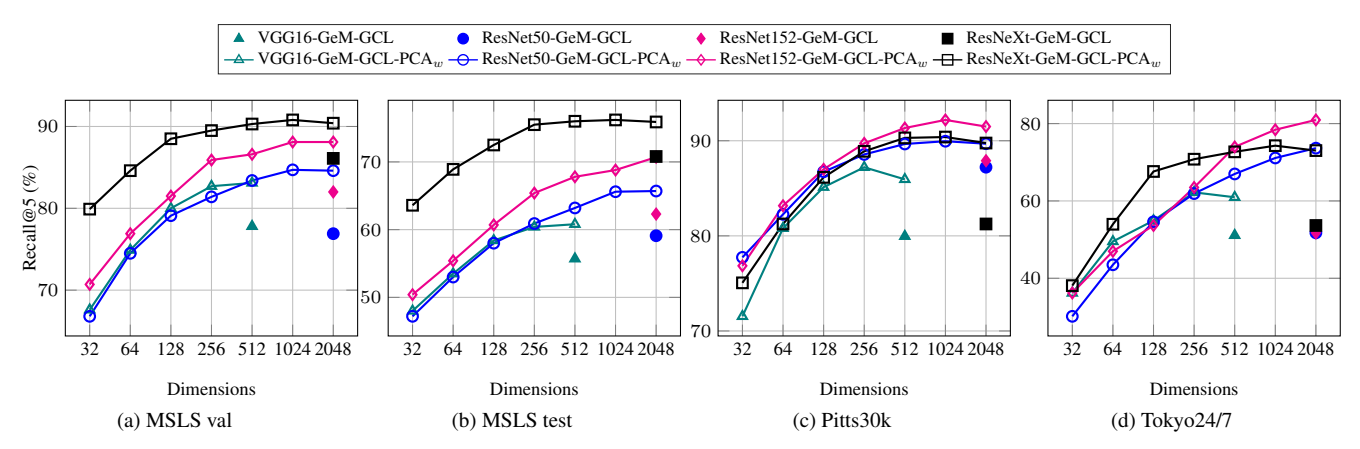


Figure 4. Ablation results on the MSLS validation, MSLS test, Pittsburgh30k and Tokyo 24/7 datasets, with different PCA dimensions.

complex NetVLAD when trained with our GCL function. We also perform whitening and PCA on the descriptors, which further boost the performance.

Ablation study: PCA and whitening. We also study the effect of whitening and PCA dimensionality reduction from 32 to 2048 dimensions. Figure 4 shows the results on the MSLS, Pittsburgh30k and Tokyo 24/7 datasets. In general, the larger the size of the descriptors, the better the results. However, our models maintain comparably high results when the descriptors are whitened and reduced to 256 dimensions, still outperforming the full-size descriptors without whitening. We observed up to a 28.2% improvement in the case of Tokyo 24/7 and 12.8% on the MSLS validation set. When comparing our VGG16-GeM-GCL model reduced to 256 dimensions with NetVLAD ($16 \times$ less descriptor size), we still achieve higher results (R@5 of 82.7% vs 80.8% on MSLS validation, 60.4% vs 58.9% on MSLS test, 87.2% vs 84.7% on Pittsburg30k and 62.2% vs 47.6% on Tokyo 24/7). It is to highlight that the contributions of the PCA/whitening and the GCL are complementary, meaning that they can be used together to optimize retrieval performance.

Comparison with other loss functions. We compared with other loss functions used for VPR, by following up on the experiments in [42]. The loss functions included in the comparison in [42] are the triplet loss [2] (also with Huber distance [41]), quadruplet loss [7], lazy triplet and lazy quadruplet loss [1], plus functions that embed mechanisms to circumvent the use of binary labels, namely a multi-similarity loss [47], log-ratio [17] and soft contrastive loss [42]. The results reported in Table 4 show that the GCL achieves higher localization accuracy especially when stricter thresholds for distance and angle are set. These results indicate that the GCL descriptors are better effective in neighbor search and retrieval, and their ranking based on distance from the query descriptor is a more reliable measure of visual place similarity. All methods in the upper part of the

		A	ll		Urba	n		Suburl	ban		Park	
Loss function	0.25m/2°	0.5m/5°	$5\text{m}/10^{\circ}$	0.25m/2°	0.5m/5°	$5\text{m}/10^{\circ}$	0.25m/2°	0.5m/5°	$5\text{m}/10^{\circ}$	0.25m/2°	0.5m/5°	5m/10°
Triplet (original NetVLAD) [2]	6.0	15.5	59.9	9.4	22.6	71.2	3.9	11.8	60.1	3.2	9.2	45.2
Quadruplet [7]	6.9	17.5	62.3	10.7	25.2	73.3	4.4	13.0	61.4	3.9	10.8	47.9
Lazy triplet [1]	6.4	16.5	58.6	9.9	23.5	69.8	4.1	11.9	58.2	3.5	10.1	42.0
Lazy quadruplet [1]	7.3	18.5	61.7	11.4	26.9	72.7	4.9	13.9	64.1	3.7	10.7	44.1
Triplet + Huber distance [41]	6.0	15.3	55.9	9.5	22.9	69.0	4.4	12.4	57.3	3.0	8.4	39.6
Log-ratio [17]	6.7	17.4	58.8	10.5	24.9	71.4	4.6	13.4	57.4	3.5	10.2	42.8
Multi-similarity [47]	7.4	18.8	66.3	12.0	28.8	81.6	5.1	14.6	63.9	3.8	10.9	52.7
Soft contrastive [42]	8.0	20.5	70.4	12.7	30.7	84.6	5.1	14.9	67.9	4.5	12.6	56.8
GCL (Ours)	9.2	22.8	65.8	14.7	34.2	82.6	5.7	16.1	64.6	5.1	14.0	49.1
GCL (Ours w/ ResNeXt)	9.9	24.3	75.5	15.4	36.0	89.6	6.7	18.4	76.8	5.6	14.9	60.3

Table 4. Comparison of localization results (on CMU Seasons) of VGG16 backbones trained with several metric loss functions. Methods in the upper part deploy a NetVLAD pooling layer.

table deploy a VGG16 backbone with a NetVLAD pooling layer and make use of hard-negative pair mining. We also use a VGG16 backbone and do not perform hard-negative pair mining, substantially reducing the training time and memory requirements. This allows us to also train backbones with larger capacity, e.g. ResNeXt, on a single V100 GPU in less than a day, of which we report the results in italics for completeness.

Processing time. The GCL function and the graded similarity labels contribute to training effective models in a dataand computation-efficient way, largely improving on the resources and time required to train NetVLAD (see Table 5). Our VGG16-GeM-GCL model obtains higher results than NetVLAD while requiring $6 \times$ less memory and about $100 \times$ less time to converge. We point out that NetVLAD is the backbone of several other methods for VPR such as Patch-NetVLAD, DELG and SuperGlue in Table 2, thus making the comparison in Table 5 relevant from a larger perspective. The graded similarity and GCL function contribute to an efficient use of training data. A single epoch, i.e. a model sees a certain training pair only once, is sufficient for the training of GCL-based models to converge. The low memory and time requirements also enable the training of models with larger backbones, that obtain very high results while still keeping the resource usage low. We point out the data-efficient training that we deployed can stimulate further and faster progress in VPR, as it enables to train larger backbones, and perform extensive hyperparameter optimization or more detailed ablation studies.

6. Conclusions

We extended the learning of image descriptors for visual place recognition by using measures of camera pose similarity and 3D surface overlap as proxies for graded image pair similarity to re-annotate existing VPR datasets (i.e. MSLS, 7Scenes and TB-Places). We demonstrated that the new labels can be used to effectively compose training batches without the need of hard-pair mining, decisively speeding-up

Model	memory	epochs	t/epoch	t/converge
NetVLAD-16-TL	9.67GB	30 (22)	24h	22d
NetVLAD-64-TL	-	10(7)	36h	10.5d
VGG16-GeM-GCL	1.49GB	1	5h	5h
ResNet50-GeM-GCL	1.65 GB	1	6h	6h
ResNet152-GeM-GCL	3.78 GB	1	14h	14h
ResNetXt-GeM-GCL	4.77 GB	1 (1/2)	28h	14h

Table 5. Training time and GPU memory utilization for a batch size of 4 images. In the epochs column, the number in parenthesis is the number of epochs until convergence.

training time while reducing memory requirements. Furthermore, we reformulated the Contrastive Loss function, proposing a Generalized Contrastive Loss (GCL). The GCL exploits the graded similarity of image pairs, and contributes to learning way better performing image descriptors for VPR than those of other losses that are not designed to use graded image similarity labels (i.e. triplet, quadruplet and their variants) and that require hard-pair mining during training. Models trained with the GCL and new graded similarity labels obtain comparable or higher results that several existing VPR methods, including those that apply re-ranking of the retrieved images, while keeping a more efficient use of the data, training time and memory. We achieved good generalization to unseen environments, showing robustness to domain shifts on the Pittsburgh30k, Tokyo 24/7, RobotCar Seasons v2 and Extended CMU Seasons datasets. The combination of graded similarity annotations and a loss function that can embed them in the training paves a way to learn more effective descriptors for VPR in a data- and resourceefficient manner.

References

- [1] Mikaela Angelina Uy and Gim Hee Lee. Pointnetvlad: Deep point cloud based retrieval for large-scale place recognition. In *CVPR*, pages 4470–4479, 2018.
- [2] Relja Arandjelovic, Petr Gronat, Akihiko Torii, Tomas Pajdla, and Josef Sivic. Netvlad: Cnn architecture for weakly

- supervised place recognition. In CVPR, pages 5297–5307, 2016.
- [3] Hernan Badino, Daniel Huber, and Takeo Kanade. The CMU Visual Localization Data Set. http://3dvis.ri.cmu.edu/data-sets/localization, 2011.
- [4] Vassileios Balntas, Shuda Li, and Victor Prisacariu. Relocnet: Continuous metric learning relocalisation using neural nets. In ECCV, pages 751–767, 2018.
- [5] Gabriele Berton, Carlo Masone, and Barbara Caputo. Rethinking visual geo-localization for large-scale applications, 2022
- [6] Bingyi Cao, André Araujo, and Jack Sim. Unifying deep local and global features for image search. In Andrea Vedaldi, Horst Bischof, Thomas Brox, and Jan-Michael Frahm, editors, ECCV 2020, pages 726–743, 2020.
- [7] Weihua Chen, Xiaotang Chen, Jianguo Zhang, and Kaiqi Huang. Beyond triplet loss: A deep quadruplet network for person re-identification. In 2017 IEEE Conference on Computer Vision and Pattern Recognition (CVPR), pages 1320–1329, 2017.
- [8] Wei Chen, Yu Liu, Weiping Wang, Erwin M. Bakker, Theodoros Georgiou, Paul W. Fieguth, Li Liu, and Michael S. Lew. Deep image retrieval: A survey. *CoRR*, abs/2101.11282, 2021.
- [9] Zetao Chen, Stephanie Lowry, Adam Jacobson, Zongyuan Ge, and Michael Milford. Distance metric learning for featureagnostic place recognition. In 2015 IEEE/RSJ International Conference on Intelligent Robots and Systems (IROS), pages 2556–2563, 2015.
- [10] Agnés Desolneux, Lionel Moisan, and Jean-Michel Morel. Gestalt theory. In From Gestalt Theory to Image Analysis: A Probabilistic Approach, pages 11–30. Springer New York, 2008
- [11] Yixiao Ge, Haibo Wang, Feng Zhu, Rui Zhao, and Hongsheng Li. Self-supervising fine-grained region similarities for largescale image localization. In Andrea Vedaldi, Horst Bischof, Thomas Brox, and Jan-Michael Frahm, editors, *Computer Vision – ECCV 2020*, pages 369–386, 2020.
- [12] Albert Gordo, Jon Almazán, Jerome Revaud, and Diane Larlus. End-to-end learning of deep visual representations for image retrieval. *International Journal of Computer Vision*, 124(2):237–254, 2017.
- [13] Raia Hadsell, Sumit Chopra, and Yann LeCun. Dimensionality reduction by learning an invariant mapping. In CVPR, volume 2, pages 1735–1742. IEEE, 2006.
- [14] Stephen Hausler, Sourav Garg, Ming Xu, Michael Milford, and Tobias Fischer. Patch-netvlad: Multi-scale fusion of locally-global descriptors for place recognition. In *CVPR*, pages 14141–14152, 2021.
- [15] Kaiming He, Xiangyu Zhang, Shaoqing Ren, and Jian Sun. Deep residual learning for image recognition. In CVPR, pages 770–778, 2016.
- [16] Sungyeon Kim, Dongwon Kim, Minsu Cho, and Suha Kwak. Embedding transfer with label relaxation for improved metric learning. In *CVPR*, pages 3967–3976, 2021.
- [17] Sungyeon Kim, Minkyo Seo, Ivan Laptev, Minsu Cho, and Suha Kwak. Deep metric learning beyond binary supervision. In CVPR, pages 2288–2297, 2019.

- [18] Maria Leyva-Vallina, Nicola Strisciuglio, Manuel López-Antequera, Radim Tylecek, Michael Blaich, and Nicolai Petkov. Tb-places: A data set for visual place recognition in garden environments. *IEEE Access*, 2019.
- [19] María Leyva-Vallina, Nicola Strisciuglio, and Nicolai Petkov. Place recognition in gardens by learning visual representations: data set and benchmark analysis. In *CAIP*, pages 324–335. Springer, 2019.
- [20] Chundi Liu, Guangwei Yu, Maksims Volkovs, Cheng Chang, Himanshu Rai, Junwei Ma, and Satya Krishna Gorti. Guided similarity separation for image retrieval. In H. Wallach, H. Larochelle, A. Beygelzimer, F. d'Alché-Buc, E. Fox, and R. Garnett, editors, Advances in Neural Information Processing Systems, volume 32, 2019.
- [21] Liu Liu, Hongdong Li, and Yuchao Dai. Stochastic attraction-repulsion embedding for large scale image localization. In CVPR, pages 2570–2579, 2019.
- [22] Manuel Lopez-Antequera, Ruben Gomez-Ojeda, Nicolai Petkov, and Javier Gonzalez-Jimenez. Appearance-invariant place recognition by discriminatively training a convolutional neural network. *Pattern Recognit. Lett.*, 92:89–95, 2017.
- [23] Stephanie Lowry, Niko Sünderhauf, Paul Newman, John J Leonard, David Cox, Peter Corke, and Michael J Milford. Visual place recognition: A survey. *IEEE Transactions on Robotics*, 32(1):1–19, 2016.
- [24] Will Maddern, Geoffrey Pascoe, Chris Linegar, and Paul Newman. 1 year, 1000 km: The oxford robotcar dataset. *Int. J. Robot. Res.*, 36(1):3–15, 2017.
- [25] Michael J Milford and Gordon F Wyeth. Seqslam: Visual route-based navigation for sunny summer days and stormy winter nights. In *ICRA*, pages 1643–1649, 2012.
- [26] Adam Paszke, Sam Gross, Soumith Chintala, Gregory Chanan, Edward Yang, Zachary DeVito, Zeming Lin, Alban Desmaison, Luca Antiga, and Adam Lerer. Automatic differentiation in pytorch. 2017.
- [27] Guohao Peng, Yufeng Yue, Jun Zhang, Zhenyu Wu, Xiaoyu Tang, and Danwei Wang. Semantic reinforced attention learning for visual place recognition. In 2021 IEEE International Conference on Robotics and Automation (ICRA), pages 13415–13422, 2021.
- [28] Noé Pion, Martin Humenberger, Gabriela Csurka, Yohann Cabon, and Torsten Sattler. Benchmarking image retrieval for visual localization. In *International Conference on 3D Vision*, 2020.
- [29] Filip Radenović, Ahmet Iscen, Giorgos Tolias, Yannis Avrithis, and Ondřej Chum. Revisiting oxford and paris: Large-scale image retrieval benchmarking. In CVPR, pages 5706–5715, 2018.
- [30] Filip Radenović, Giorgos Tolias, and Ondřej Chum. Finetuning cnn image retrieval with no human annotation. *TPAMI*, 41(7):1655–1668, 2018.
- [31] Jerome Revaud, Jon Almazán, Rafael S Rezende, and Cesar Roberto de Souza. Learning with average precision: Training image retrieval with a listwise loss. In *ICCV*, pages 5107– 5116, 2019.
- [32] Paul-Edouard Sarlin, Daniel DeTone, Tomasz Malisiewicz, and Andrew Rabinovich. SuperGlue: Learning feature matching with graph neural networks. In *CVPR*, 2020.

- [33] Torsten Sattler, Will Maddern, Carl Toft, Akihiko Torii, Lars Hammarstrand, Erik Stenborg, Daniel Safari, Masatoshi Okutomi, Marc Pollefeys, Josef Sivic, et al. Benchmarking 6dof outdoor visual localization in changing conditions. In *CVPR*, pages 8601–8610, 2018.
- [34] Torsten Sattler, Tobias Weyand, Bastian Leibe, and Leif Kobbelt. Image retrieval for image-based localization revisited. In BMVC, volume 1, page 4, 2012.
- [35] Torsten Sattler, Qunjie Zhou, Marc Pollefeys, and Laura Leal-Taixé. Understanding the limitations of cnn-based absolute camera pose regression. In 2019 IEEE/CVF Conference on Computer Vision and Pattern Recognition (CVPR), pages 3297–3307, 2019.
- [36] Johannes Lutz Schönberger and Jan-Michael Frahm. Structure-from-motion revisited. In *Conference on Computer Vision and Pattern Recognition (CVPR)*, 2016.
- [37] Hailin Shi, Yang Yang, Xiangyu Zhu, Shengcai Liao, Zhen Lei, Weishi Zheng, and Stan Z Li. Embedding deep metric for person re-identification: A study against large variations. In ECCV, pages 732–748. Springer, 2016.
- [38] Jamie Shotton, Ben Glocker, Christopher Zach, Shahram Izadi, Antonio Criminisi, and Andrew Fitzgibbon. Scene coordinate regression forests for camera relocalization in rgbd images. In CVPR, pages 2930–2937, 2013.
- [39] Karen Simonyan and Andrew Zisserman. Very deep convolutional networks for large-scale image recognition. *ICLR*, 2015.
- [40] Nicola Strisciuglio, Radim Tylecek, Michael Blaich, Nicolai Petkov, Peter Biber, Jochen Hemming, Eldert van Henten, Torsten Sattler, Marc Pollefeys, Theo Gevers, et al. Trimbot2020: an outdoor robot for automatic gardening. In *ISR*, pages 1–6. VDE, 2018.
- [41] Janine Thoma, Danda Pani Paudel, Ajad Chhatkuli, and Luc Van Gool. Geometrically mappable image features. *IEEE Robotics and Automation Letters*, 5(2):2062–2069, 2020.
- [42] Janine Thoma, Danda P Paudel, and Luc Van Gool. Soft contrastive learning for visual localization. *NeurIPS*, 2020.
- [43] A. Torii, R. Arandjelović, J. Sivic, M. Okutomi, and T. Pajdla. 24/7 place recognition by view synthesis. In *CVPR*, 2013.
- [44] A. Torii, J. Sivic, M. Okutomi, and T. Pajdla. Visual place recognition with repetitive structures. *TPAMI*, 2015.
- [45] Laurens Van der Maaten and Geoffrey Hinton. Visualizing data using t-sne. *J. Mach. Learn. Res.*, 9(11), 2008.
- [46] Ruotong Wang, Yanqing Shen, Weiliang Zuo, Sanping Zhou, and Nanning Zhen. Transvpr: Transformer-based place recognition with multi-level attention aggregation. In *CVPR*, 2022.
- [47] Xun Wang, Xintong Han, Weilin Huang, Dengke Dong, and Matthew R. Scott. Multi-similarity loss with general pair weighting for deep metric learning. In 2019 IEEE/CVF Conference on Computer Vision and Pattern Recognition (CVPR), pages 5017–5025, 2019.
- [48] Frederik Warburg, Søren Hauberg, Manuel López-Antequera, Pau Gargallo, Yubin Kuang, and Javier Civera. Mapillary street-level sequences: A dataset for lifelong place recognition. In CVPR, 2020.
- [49] Tobias Weyand, Andre Araujo, Bingyi Cao, and Jack Sim. Google landmarks dataset v2-a large-scale benchmark for

- instance-level recognition and retrieval. In CVPR, pages 2575–2584, 2020.
- [50] Saining Xie, Ross Girshick, Piotr Dollár, Zhuowen Tu, and Kaiming He. Aggregated residual transformations for deep neural networks. In CVPR, pages 1492–1500, 2017.
- [51] Mubariz Zaffar, Sourav Garg, Michael Milford, Julian Kooij, David Flynn, Klaus McDonald-Maier, and Shoaib Ehsan. Vpr-bench: An open-source visual place recognition evaluation framework with quantifiable viewpoint and appearance change. *International Journal of Computer Vision*, 129(7):2136–2174, 2021.

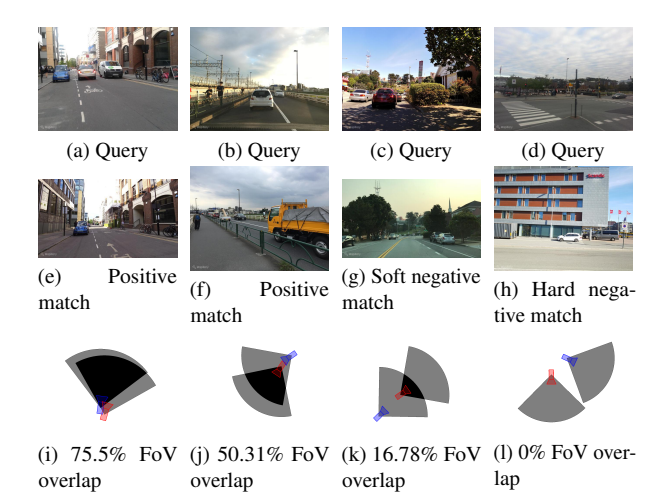


Figure 5. Example image pairs from the MSLS dataset. The first row shows the query images, the second row shows the corresponding matches from the map set, and the third row shows the estimated 2D FoV overlap. The query image is associated with the red camera, while the map image with the blue camera. The first column shows a positive match with 75.5% FoV overlap, and many visual features in common. The second column shows a borderline pair: the two images have 50.31% FoV overlap and some features in common. The third column shows a soft negative match, where the two images have FoV overlap of 16.78%. The fourth column shows a hard negative match, where the two images are taken by cameras looking in opposite directions, and the FoV overlap is 0%.

A. Implementation and training details.

We carried out experiments using PyTorch [26] and a single Nvidia V100 GPU. For all considered backbones (pretrained on ImageNet), we trained the two last convolutional blocks for one epoch only on the MSLS train set (\sim 500k pairs), making an efficient use of training data. We use the SGD optimizer with initial learning rate of 0.1 for the runs with the GCL function and 0.01 for those with the CL function, and decrease it by a factor of 10^{-1} after 250k pairs. For the TB.Places and 7Scene experiments, since they are much smaller datasets we train for 30 epochs, reaching convergence around epoch 15 for both datasets. The initial learning rate is the same as we used for the MSLS experiments, and we decrease it by a factor of 10^{-1} after every 5 epochs. All the descriptors are L2-normalized.

B. Relabeling with image similarity proxies

2D Field of View Overlap: MSLS data set The authors of MSLS defined a positive match when the retrieved map image falls within 25m and 40° from the query. We define a similarity measure that satisfies those constraints. Image pairs taken at locations that are closer than 25m and with orientation differences lower than 40° are expected to have a similarity higher than 50%, to be considered similar. More-



Figure 6. Example image pairs from the TB-Places dataset. The first row shows a positive pair with FoV overlap of 74%. The second row depicts a soft negative pair with FoV overlap equal to 41%. The red camera corresponds to the query image, while the blue one to the map image.

over, the borderline cases with distances close to 25m and/or orientation difference near to 40° should have a similarity close to 50%. Hence, we define $r=25m\times 2=50m$ and estimate a θ that gives approximately a 50% FoV overlap for the borderline cases, i.e. $0\text{m}@40^\circ$, and $25\text{m}@0^\circ$. For the former, the optimal θ corresponds to 80° , and for the second latter to 102° . We settle for a value in the middle and define $\theta=90^\circ$, which gives 55.63% and 45.01% FoV overlaps in the borderline cases. We display examples of the similarity ground truth for MSLS in Fig. 5. We compute the similarity ground truth for each possible query-map pair, per city. The new annotations are publicly available.

2D Field of View Overlap with IMU and laser tracking: TB-Places dataset We present another computation of the 2D field of View overlap to estimate the similarity of image pairs when 6DOF camera pose information is available as metadata next to the images in the dataset. The translation vector (t_0, t_1) and orientation angle α are extracted from the pose vector.

This is the case of the TB-Places dataset [18], for visual place recognition in gardens, created for the Trimbot2020 project [40]. It contains images taken in an experimental garden over three years and includes variations in illumination, season and viewpoint. Each image comes with a 6DOF camera pose, obtained with an IMU and laser tracking, which allows us to estimate a very precise 2D FoV. According to the original paper of the TB-places dataset, we set the FoV angle of the cameras as $\theta=90^\circ$ and the radius as r=3.5m. We thus estimate the 2D field of view overlap and use it to re-label the pairs of images contained in the dataset. We provide the similarity ground truth for all possible pairs within W17, the training set. We show some examples of image pairs and their 2D FoV overlap in Fig. 6.

3D Surface Overlap: 7Scenes dataset

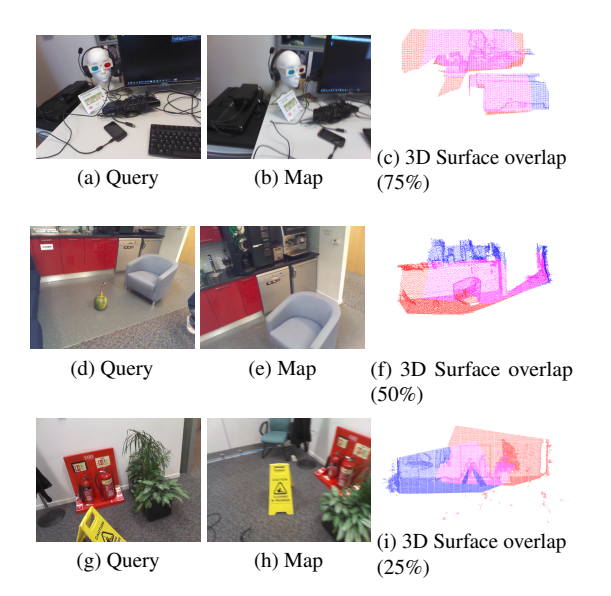


Figure 7. 3D Surface overlap examples from the 7Scenes dataset. The first row shows a positive pair with 3D Surface overlap of 75%. The second row depicts a borderline pair with 50% 3D Surface overlap. The last row shows a soft negative image pair with 25% 3D Surface overlap. The red pointcloud corresponds to the query 3D Surface, the blue one is the map, and the magenta represents the overlap between them.

When the 3D reconstruction of a concerned environment is available, we estimate the degree of similarity of image pairs by computing the 3D Surface overlap. We project a given image with an associated 6DOF camera pose onto the reconstructed pointcloud of the environment. We select the subset of 3D points that falls within the boundaries of the image as the image 3D Surface. For an image pair, we compute their 3D Surface overlap as the intersection-overunion (IoU) of the sets of 3D points associated with the two images. This computation is similar to the maximum inliers measure proposed in [30], where it was used as part of a pair-mining strategy that also involved the computation of a distance in the latent space. We consider, instead, the computed 3D Surface overlap as a proxy for the degree of similarity of a pair of images.

We use the 3D Surface overlap to re-annotate the 7Scenes dataset [38], an indoor localization benchmark, that contains RGBD images taken in seven environments. Each image has an associated 6DOF pose, and a 3D reconstruction of each scene is available. We provide annotations for each possible pair within the training set per scene. We show some examples of the 3D Surface overlap in Fig. 7. We display the 3D Surface associated to the query image in red, that of the map image in blue and their overlap in magenta.

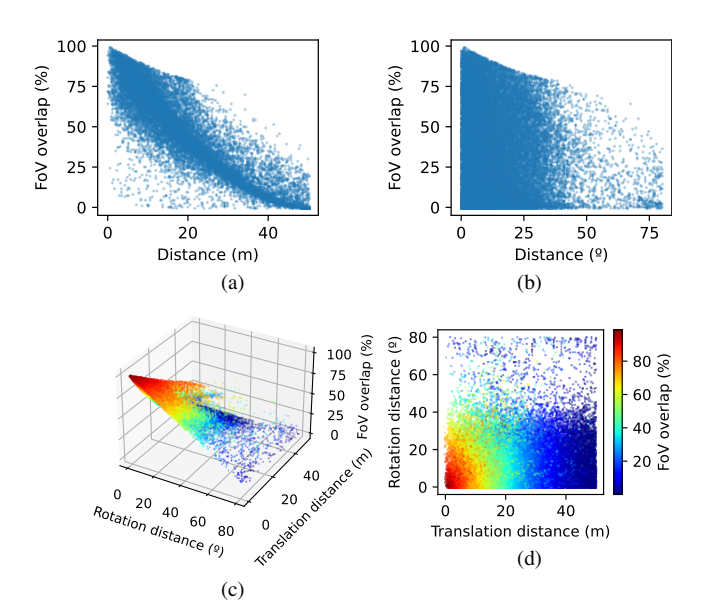


Figure 8. Relation of 2D FoV overlap with translation and orientation distance (computed using a subset of MSLS validation set).

B.1. Field of View vs. Distance

We studied the relation among translation distance, rotation difference and the resulting FoV overlap measure. For that, we selected a subset of pairs of the MSLS training set and measured how the value of the FoV overlap varies with respect to the position and orientation difference of the image pairs. In Fig. 8a, we plot the relationship between the translation distance and the value of the FoV overlap. We observed a somewhat linear relationship between increasing translation distance and decreasing FoV overlap. Moreover, many image pairs with FoV overlap of approximately 50% were taken at a distance of about 25m. The variance observed in Fig. 8a is attributable to the orientation changes. Indeed, the relation between FoV overlap and orientation difference is less clear (see Fig. 8b). However, the pairs with smaller orientation distance tend to have a generally higher FoV overlap. We plot the relation of the FoV overlap with both translation and orientation distance in a 3-dimensional plane in Fig. 8c, and as a heatmap in Fig. 8d. Rotation and translation distance jointly influence the FoV overlap: the smaller the translation and orientation distance, the higher the similarity. Furthermore, the higher one of the distance measures, the lower the computed FoV overlap, and thus the annotated ground truth similarity.

C. CL vs GCL: comparison of latent space

In Fig. 9, we show the 2D projection of the difference of the latent space representations of 2000 image pairs (1000 positive and 1000 negative) randomly selected from the

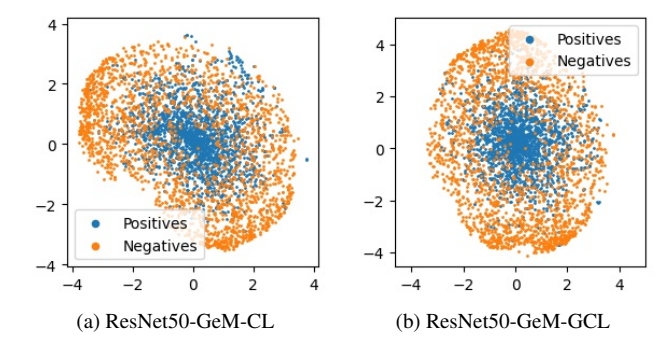


Figure 9. Visualization of the learned latent space. We selected 1000 random positive pairs and 1000 random negative pairs from the MSLS Copenhagen set, computed the differences between their representations and projected them into a 2D space using t-SNE.

Copenhagen set of the MSLS validation set. For each pair, we compute the difference between the map and the query image descriptors. We use this as input to t-SNE [45], which projects the descriptors onto a 2D space. We visualize the vectors produced by two models with a ResNet50-GeM backbone, one trained using the CL function (Fig. 9a) and the other using the GCL (Fig. 9b) function. The effect of the proposed GCL function is evident in the better regularized latent space, where the representation of similar image pairs (blue dots) are more consistently distributed towards the center of the space. The representations learned using the CL function, instead, form a more scattered and noisy distribution.

D. Large-scale VPR: additional results

D.1. RobotCar Seasons v2 and Ext. CMU Seasons

We provide results divided by type of environment for the Extended CMU dataset in Table 6. We observed that all models (ours and SoTA) tend to reach a higher performance on the urban images. This is logical, as they are all trained on the MSLS dataset with images of mainly urban areas.

We also provide detailed results for the RobotCar Seasons v2 dataset, organized by weather and illumination conditions, in Table 7. We observe that all methods obtain a higher successful localization rate on day conditions, and the GCL-based methods (especially with a ResNet backbone) tend to have goof performance on the night-time subsets as well. The MSLS train dataset includes images taken at night, although underrepresented, so it is interesting that GCL based models can localize images under these conditions.

D.2. Results on Pittsburgh250k and TokyoTM

We evaluated the generalization of our models trained on MSLS to the Pittsburgh250k [44] and TokyoTM [2] datasets. The test set of the former consists of 83k map and 8k query images taken over the span of several years in Pittsburgh, Pennsylvania, USA. The TokyoTM dataset consists of im-

		** *		
Method	Mean 0.25/0.5/10m 2/5/10°	Urban 0.25/0.5/10m 2/5/10°	Suburban 0.25/0.5/10m 2/5/10°	Park 0.25/0.5/10m 2/5/10°
NetVLAD-64	1.3 / 4.5 / 31.9	2.9 / 8.4 / 49.6	0.8 / 3.4 / 29.7	0.3 / 1.6 / 15.2
NetVLAD-64*	3.9 / 12.1 / 58.4	7.6 / 20.3 / 77.2	2.6 / 9.7 / 58.9	1.6 / 6.3 / 37.0
NetVLAD-16	1.7 / 5.5 / 39.1	3.7 / 10.0 / 57.3	1.1 / 4.5 / 38.6	0.4 / 1.9 / 19.8
NetVLAD-16*	4.4 / 13.7 / 61.4	8.4 / 22.1 / 76.9	3.0 / 11.4 / 63.1	1.9 / 7.4 / 41.9
VGG-avg-CL	0.9 / 3.0 / 22.7	2.0 / 5.8 / 39.4	0.6 / 2.3 / 21	0.2 / 0.7 / 6.5
VGG-avg-GCL	2.3 / 7.2 / 43.3	4.7 / 13.0 / 64.3	1.6 / 5.8 / 43.4	0.7 / 2.5 / 19.8
VGG-avg-CL*	2.1 / 6.6 / 34.9	4.4 / 12.3 / 54.1	1.1 / 4.4 / 30.5	0.9 / 3.1 / 19.4
VGG-avg-GCL*	3.7 / 11.2 / 52.5		2.1 / 8.2 / 50.4	1.8 / 6.2 / 35.1
VGG-GeM-CL	2.8 / 8.6 / 44.5	5.7 / 15.2 / 63.7	1.6 / 6.4 / 44.9	1.1 / 4.2 / 22.8
VGG-GeM-GCL		6.8 / 18.5 / 73.6	2.5 / 9.2 / 57.3	1.5 / 5.6 / 34.2
VGG-GeM-CL*		8.4 / 21.5 / 72.1	2.6 / 10 / 55.2	2.3 / 8.7 / 40.8
VGG-GeM-GCL*	5.7 / 17.1 / 66.3	10.4 / 26.8 / 82.2	3.8 / 13.8 / 67.8	2.8 / 10.7 / 46.7
ResNet50-avg-CL	2.6 / 7.8 / 43.4	5.6 / 14.9 / 64.6	1.4 / 5.5 / 42.6	0.8 / 2.9 / 21.1
ResNet50-avg-GCL	3.1 / 9.7 / 55.1	6 / 16.7 / 73.6	2.0 / 7.7 / 56.8	1.2 / 4.7 / 32.5
ResNet50-avg-CL*	4.7 / 13.8 / 50.8	9.5 / 24.1 / 70.5	2.7 / 9.7 / 48.8	2.1 / 7.6 / 31.7
ResNet50-avg-GCL*	5.4 / 16.2 / 66.5	10.2 / 26.5 / 81.8	3.5 / 12.5 / 69.8	2.6 / 9.6 / 45.3
ResNet50-GeM-CL	3.2 / 9.6 / 49.5	6.5 / 17.3 / 70.7	1.9 / 7.0 / 49.3	1.2 / 4.3 / 26.3
ResNet50-GeM-GCL	3.8 / 11.8 / 61.6	7.4 / 19.9 / 79.2	2.4 / 9.4 / 64.8	1.5 / 6.1 / 38.1
ResNet50-GeM-CL*		9.5 / 23.9 / 73.5	2.8 / 9.6 / 49.7	1.9 / 6.8 / 30.0
ResNet50-GeM-GCL*	5.4 / 16.5 / 69.9	10.1 / 26.3 / 84.5	3.5 / 13.4 / 74.1	2.6 / 9.8 / 48.2
ResNet152-avg-CL	3.0 / 9.2 / 49.9	6.2 / 16.4 / 70.4	1.9 / 6.9 / 48.7	1.0 / 4.1 / 28.9
ResNet152-avg-GCL		7.0 / 18.9 / 78.8	2.3 / 8.4 / 62.6	1.4 / 5.5 / 39.9
ResNet152-avg-CL*	4.8 / 14.3 / 59.9		3.0 / 10.9 / 61	2/8/39.3
ResNet152-avg-GCL*	5.7 / 17.0 / 66.5	10.8 / 27.3 / 82.0	3.7 / 13.5 / 68.9	
ResNet152-GeM-CL	3.2 / 9.7 / 52.2	6.7 / 17.7 / 73.9	2.1 / 7.3 / 52.8	0.9 / 4.1 / 27.6
ResNet152-GeM-GCL		6.9 / 18.8 / 79.3	2.5 / 9.0 / 64.3	1.3 / 6.0 / 43.6
ResNet152-GeM-CL*		9.6 / 24.5 / 75.2	3.0 / 10.5 / 54.3	
ResNet152-GeM-GCL*	5.3 / 16.1 / 66.4	9.9 / 25.8 / 81.6	3.5 / 12.8 / 69.3	2.4 / 9.7 / 46
ResNext-avg-CL	2.0 / 6.1 / 40.0	4.6 / 12.2 / 63.6	1.2 / 4.4 / 38.5	0.3 / 1.7 / 16.0
ResNext-avg-GCL		6.7 / 17.9 / 77.8	2.1 / 8.1 / 58.1	1.2 / 4.4 / 35.0
ResNext-avg-CL*	4.6 / 13.4 / 58.6	9.3 / 23.2 / 78	2.8 / 10.1 / 59	1.7 / 6.7 / 36.5
ResNext-avg-GCL*		10.4 / 26.6 / 85.1		
ResNext-GeM-CL	2.9 / 9.0 / 52.6	5.9 / 15.6 / 70.2	1.7 / 6.8 / 53.0	1.2 / 4.7 / 32.6
ResNext-GeM-GCL	3.5 / 10.5 / 58.8	6.5 / 17.7 / 77.8	2.5 / 8.7 / 59.7	1.3 / 5.0 / 36.6
ResNext-GeM-CL*	4.9 / 14.4 / 61.7	9.4 / 24 / 80.2	3.1 / 11.1 / 63.8	
ResNext-GeM-GCL*	6.1 / 18.2 / 74.9	11.1 / 28.7 / 87.4	4.2 / 14.6 / 77.4	3.1 / 11.1 / 57.7

Table 6. Detailed results on the Extended CMU dataset. The denotes the models for which PCA whitening has been applied.

ages collected using the Time Machine tool on Google Street View in Tokyo over several years. Its validation set is divided into a map and a query set, with 49k and 7k images.

The results (see Table 8) are in line with those reported in the main paper. Our models trained with a GCL function generalize better to unseen datasets than their counterpart trained with a binary Contrastive Loss. Their performance is further boosted if PCA whitening is applied, up to a top-5 recall of 93.7% on Pittsburgh250k and 96.7% on TokyoTM.

E. Additional ablations

E.1. Average pooling and PCA

In addition to using GeM, we trained the considered backbones (i.e. VGG16, ResNet50, ResNet152 and ResNeXt) using a Global Average Pooling layer on the MSLS dataset. We show the results in Table 9. We observed that our method can reach good results also with a simple pooling layer, although a GeM layer usually leads to better results (see main paper). Our methods reach good results on the validation and test sets of MSLS and generalizes well to unseen datasets such as Pittsburgh30k [2], Tokyo24/7 [2], RobotCar Seasons

Method	night rain 0.25/0.5/10m 2/5/10°	night 0.25/0.5/10m 2/5/10°	night all 0.25/0.5/10m 2/5/10°	overcast winter 0.25/0.5/10m 2/5/10°	sun 0.25/0.5/10m 2/5/10°	rain 0.25/0.5/10m 2/5/10°	snow 0.25/0.5/10m 2/5/10°	dawn 0.25/0.5/10m 2/5/10°	dusk 0.25/0.5/10m 2/5/10°	overcast summer 0.25/0.5/10m 2/5/10°	day all 0.25/0.5/10m 2/5/10°	mean 0.25/0.5/10m 2/5/10°
NetVLAD-64	0.5 / 1.0 / 5.9	0.0 / 0.4 / 4.4	0.2/0.7/5.1	0.0 / 11.6 / 67.7		4.4 / 22.0 / 91.2	4.7 / 13.0 / 60.5		2.5 / 14.2 / 78.7	1	2.5 / 11.7 / 57.5	2/9.2/45.5
NetVLAD-64*	0.0 / 1.5 / 11.8	0.0 / 1.3 / 12.4	0.0 / 1.4 / 12.1	0.0 / 15.2 / 87.2		8.8 / 35.6 / 99.0	7.0 / 28.4 / 90.2		4.1 / 25.4 / 98.0		5.5 / 22.9 / 84.7	4.2 / 18 / 68.1
NetVLAD-16	0.0 / 0.0 / 3.4	0.0 / 0.9 / 5.3	0.0 / 0.5 / 4.4	1.2 / 10.4 / 78.0		5.9 / 25.4 / 93.7	3.3 / 10.7 / 62.8		1.5 / 16.2 / 86.8		2.3 / 11.8 / 61.5	
NetVLAD-16*	0.0 / 0.0 / 1.0	0.0 / 0.9 / 7.1	0.0 / 0.5 / 4.2	1.8 / 19.5 / 90.2							6.2 / 23.1 / 83.6	
VGG-avg-CL	0.0 / 0.0 / 2.5	0.0 / 0.0 / 1.3	0.0 / 0.0 / 1.9	0.0 / 7.9 / 54.9	0.0 / 2.2 / 14.3	4.9 / 23.9 / 85.4	3.3 / 8.8 / 49.8	0.9 / 1.3 / 14.5	0.0 / 12.2 / 66.5	0.0 / 3.3 / 31.8	1.3 / 8.3 / 44.0	1/6.4/34.4
VGG-avg-GCL	0.0 / 0.5 / 3.9	0.0 / 0.0 / 1.8	0.0 / 0.2 / 2.8	0.6 / 15.2 / 82.9	2.2 / 6.7 / 44.6	7.8 / 31.7 / 95.1	4.2 / 19.5 / 73.0		2.0 / 21.8 / 86.3		3.0 / 16.1 / 66.3	2.3 / 12.5 / 51.7
VGG-avg-CL*	0.0 / 0.0 / 0.0	0.0 / 0.0 / 0.0	0.0 / 0.0 / 0.0	0.0 / 11.0 / 61.6	0.4 / 4.0 / 20.5	5.9 / 26.3 / 85.4	5.1 / 13.5 / 64.2	3.1 / 8.4 / 40.1	4.1 / 17.3 / 76.6	1.9 / 11.8 / 40.3	3.0 / 13.0 / 54.5	2.3 / 10 / 42
VGG-avg-GCL*	0.0 / 0.0 / 1.0	0.0 / 0.0 / 0.4	0.0 / 0.0 / 0.7	0.6 / 17.1 / 79.3	3.1 / 11.2 / 49.1	9.3 / 34.6 / 97.6	6.5 / 17.7 / 80.0	3.5 / 16.3 / 56.4	5.6 / 25.4 / 90.9	3.8 / 18.0 / 69.7	4.7 / 19.9 / 73.9	3.6 / 15.3 / 57.1
VGG-GeM-CL	0.0 / 0.0 / 2.0	0.0 / 0.4 / 1.8	0.0 / 0.2 / 1.9	0.0 / 14.6 / 80.5	2.2 / 6.7 / 45.5	8.3 / 31.2 / 94.1	6.0 / 20.0 / 77.7	3.5 / 11.5 / 47.1	2.0 / 17.8 / 89.8	4.7 / 18.0 / 68.2	4.0 / 17.0 / 70.8	3.1 / 13.2 / 55
VGG-GeM-GCL	0.0 / 0.5 / 7.4	0.0 / 0.0 / 0.9	0.0 / 0.2 / 4.0	0.6 / 16.5 / 82.3	2.2 / 11.6 / 61.2	10.2 / 38.0 / 99.0	7.9 / 23.3 / 83.7	2.6 / 11.5 / 51.1	2.0 / 22.3 / 90.9	7.1 / 20.9 / 70.6	4.8 / 20.4 / 76.2	3.7 / 15.8 / 59.7
VGG-GeM-CL*	0.0 / 0.5 / 2.0	0.0 / 0.0 / 0.0	0.0 / 0.2 / 0.9	0.6 / 18.9 / 84.8	2.7 / 13.4 / 60.3	8.3 / 36.6 / 98.5	8.4 / 27.0 / 85.1	6.6 / 22.5 / 70.5	5.6 / 29.9 / 95.9	4.7 / 21.3 / 74.9	5.4 / 24.2 / 80.8	4.2 / 18.7 / 62.5
VGG-GeM-GCL*	0.5 / 1.0 / 6.4	0.0 / 1.3 / 6.6	0.2 / 1.2 / 6.5	1.2 / 23.2 / 90.9	6.7 / 21.4 / 78.1	11.2 / 42.4 / 100.0	9.3 / 32.6 / 95.3	7.5 / 20.7 / 76.7	4.6 / 28.9 / 97.5	6.2 / 27.0 / 79.6	6.9 / 28.0 / 87.9	5.4 / 21.9 / 69.2
ResNet50-avg-CL	0.5 / 1.0 / 9.4	0.4 / 2.2 / 11.1	0.5 / 1.6 / 10.3	0.0 / 13.4 / 71.3	1.8 / 6.2 / 30.4	8.8 / 32.7 / 97.6	5.6 / 18.6 / 64.7	4.4 / 15.4 / 53.7	3.0 / 14.7 / 79.2	2.8 / 10.4 / 51.7	3.9 / 15.9 / 63.1	3.1 / 12.6 / 51
ResNet50-avg-GCL	1.0 / 2.0 / 12.8	0.4 / 1.3 / 8.4	0.7 / 1.6 / 10.5	0.6 / 18.3 / 80.5	1.3 / 6.7 / 43.8	8.3 / 34.1 / 96.1	4.7 / 15.3 / 72.6	2.6 / 11.0 / 51.1	2.0 / 16.2 / 88.8	4.3 / 14.2 / 64.0	3.5 / 16.3 / 69.9	2.9 / 12.9 / 56.3
ResNet50-avg-CL*	0.0 / 0.0 / 3.0	0.0 / 0.4 / 1.8	0.0 / 0.2 / 2.3	2.4 / 26.2 / 89.6	3.6 / 14.3 / 53.1	14.6 / 45.4 / 98.0	8.4 / 30.7 / 84.2	10.1 / 31.7 / 75.3	5.6 / 24.9 / 93.4	7.6 / 33.6 / 76.8	7.6 / 29.5 / 80.7	5.9 / 22.8 / 62.7
ResNet50-avg-GCL*	0.0 / 1.0 / 6.4	0.4 / 0.4 / 10.2	0.2 / 0.7 / 8.4	3.0 / 28.0 / 98.2	4.0 / 15.6 / 68.8	13.2 / 41.5 / 97.6	8.4 / 31.2 / 87.9	8.4 / 30.4 / 84.1	5.6 / 27.9 / 96.4	9.5 / 33.6 / 86.3	7.6 / 29.7 / 87.8	5.9 / 23.1 / 69.6
ResNet50-GeM-CL	0.5 / 1.5 / 11.8	0.4 / 1.3 / 8.0	0.5 / 1.4 / 9.8	0.0 / 16.5 / 82.9		9.8 / 33.7 / 97.1			1.5 / 19.8 / 93.4	6.2 / 18.5 / 64.9	4.0 / 19.5 / 76.9	
ResNet50-GeM-GCL	0.5 / 2.0 / 9.9	0.0 / 1.3 / 11.9	0.2 / 1.6 / 11.0	1.8 / 21.3 / 84.8			5.1 / 18.1 / 80.9		2.0 / 17.8 / 91.9		3.7 / 17.7 / 73.4	
ResNet50-GeM-CL*	0.5 / 0.5 / 3.9	0.0 / 0.4 / 2.7	0.2 / 0.5 / 3.3	3.0 / 28.0 / 95.1				7.0 / 23.8 / 83.7			6.4 / 27.2 / 85.3	
ResNet50-GeM-GCL*	0.0 / 0.0 / 8.4	0.0 / 0.0 / 9.3	0.0 / 0.0 / 8.9	3.0 / 25.6 / 95.7	3.1 / 14.7 / 69.2	9.3 / 34.6 / 98.0	6.5 / 28.4 / 90.7	9.3 / 28.6 / 86.3	3.6 / 25.9 / 96.4	7.1 / 26.1 / 83.9	6.1 / 26.2 / 88.1	4.7 / 20.2 / 70
ResNet152-avg-CL	0.0 / 0.0 / 8.4	0.0 / 0.0 / 8.0	0.0 / 0.0 / 8.2	1.2 / 17.1 / 86.0				2.6 / 11.9 / 53.3			3.3 / 17.0 / 71.0	
ResNet152-avg-GCL	0.0 / 1.5 / 11.3		0.2 / 0.9 / 10.7	1.8 / 20.1 / 90.2	3.6 / 8.5 / 52.7	9.3 / 29.3 / 95.6		2.6 / 12.8 / 47.6			4.2 / 17.3 / 74.5	
ResNet152-avg-CL*		4.3 / 13.6 / 57.6		2.0 / 8.0 / 39.3		4.9 / 14.2 / 58.1		4.5 / 13.3 / 55.1			5.5 / 16.2 / 67.2	
ResNet152-avg-GCL*			10.8 / 27.3 / 82.0			5.7 / 16.8 / 63.1			6.1 / 19.6 / 74.9		6.2 / 18.5 / 73.6	
ResNet152-GeM-CL		3.0 / 9.8 / 53.9	6.7 / 17.7 / 73.9	0.9 / 4.1 / 27.6	3.2 / 8.9 / 52.2	3.3 / 9.2 / 47.4	3.1 / 8.9 / 47.9		3.4 / 11.5 / 61.0		3.7 / 11.0 / 56.3	
ResNet152-GeM-GCL		3.3 / 11.0 / 63.8			4.1 / 11.4 / 62.9	3.5 / 11.2 / 58.9			3.6 / 12.6 / 70.4		3.8 / 11.9 / 68.4	
ResNet152-GeM-CL*		4.4 / 13.6 / 53.2			4.9 / 13.4 / 53.9	5.0 / 14.1 / 53.5		4.4 / 12.9 / 50.0			5.5 / 15.9 / 62.2	
ResNet152-GeM-GCL*		1	9.9 / 25.8 / 81.6	1				5.1 / 15.6 / 63.7			6.1 / 17.9 / 74.0	
ResNext-avg-CL		0.0 / 1.3 / 15.5	0.5 / 2.3 / 21.9	1.2 / 12.8 / 86.0			6.5 / 16.7 / 80.0		2.5 / 17.8 / 84.8		3.4 / 13.5 / 72.6	
ResNext-avg-GCL	0.0 / 0.5 / 11.8		0.0 / 0.7 / 14.0			6.8 / 25.4 / 96.6		2.6 / 11.9 / 63.4			3.5 / 15.9 / 77.7	
ResNext-avg-CL*		0.0 / 0.9 / 12.8	0.5 / 1.2 / 12.6	0.6 / 25.6 / 97.6		9.3 / 35.1 / 99.0			5.6 / 24.9 / 94.4		6.1 / 26.1 / 87.9	
ResNext-avg-GCL*	1.0 / 3.4 / 29.1	0.0 / 1.3 / 15.5	0.5 / 2.3 / 21.9	1.2 / 12.8 / 86.0		6.8 / 20.5 / 97.6	6.5 / 16.7 / 80.0		2.5 / 17.8 / 84.8		3.4 / 13.5 / 72.6	
ResNext-GeM-CL	0.0 / 1.5 / 6.9	0.0 / 0.4 / 8.0	0.0 / 0.9 / 7.5	0.0 / 17.1 / 82.3		3.9 / 20.5 / 96.6	3.7 / 12.6 / 74.9		2.0 / 21.3 / 90.4		2.4 / 13.2 / 68.9	
ResNext-GeM-GCL			0.2 / 1.9 / 21.0	1.2 / 15.2 / 84.8		7.3 / 28.3 / 98.5			4.1 / 20.8 / 90.9		3.5 / 16.8 / 78.4	
ResNext-GeM-CL*			0.2 / 1.2 / 11.2		4.9 / 15.6 / 79.0			3.5 / 15.0 / 67.0			4.9 / 21.9 / 85.1	
ResNext-GeM-GCL*	2.5 / 5.4 / 38.4	1.8 / 3.5 / 28.3	2.1 / 4.4 / 33.1	1.2 / 26.8 / 93.9	3.6 / 15.2 / 77.2	9.8 / 40.0 / 98.5	[7.9 / 29.3 / 91.2	4.8 / 19.8 / 82.4	5.1 / 25.9 / 92.9	5.7 / 26.1 / 76.8	5.5 / 25.9 / 87.1	4.7 / 21 / 74.7

Table 7. Detailed results on the RobotCar Seasons v2 dataset, divided by wheather and ilumination conditions. The symbol * denotes the models for which PCA whitening has been applied.

			Pit	tsburgh	250k	1	TokyoTN	1
Method	PCA_w	Dim	R@1	R@5	R@10	R@1	R@5	R@10
VGG-avg-CL	No	512	20.2	38.0	47.2	38.9	58.5	67.2
VGG-avg-GCL	No	512	32.1	53.4	62.7	65.6	80.8	85.2
VGG-avg-CL	Yes	128	39.3	58.9	67.4	66.0	80.3	85.0
VGG-avg-GCL	Yes	256	51.3	71.0	78.0	78.6	87.7	90.8
VGG-GeM-CL	No	512	44.5	63.1	70.1	67.7	80.8	85.0
VGG-GeM-GCL	No	512	53.3	72.4	79.2	75.5	85.4	88.6
VGG-GeM-CL	Yes	512	65.1	81.2	85.8	83.7	91.1	93.3
VGG-GeM-GCL	Yes	512	73.4	86.4	89.9	88.2	93.2	94.7
ResNet50-avg-CL	No	2048	45.1	65.8	73.6	69.7	83.0	87.5
ResNet50-avg-GCL	No	2048	56.2	77.1	83.8	72.3	84.8	88.4
ResNet50-avg-CL	Yes	2048	70.6	85.4	89.5	90.5	94.8	96.0
ResNet50-avg-GCL	Yes	1024	74.6	87.9	91.6	91.7	95.7	96.8
ResNet50-GeM-CL	No	2048	54.8	74.2	80.7	73.3	85.4	89.2
ResNet50-GeM-GCL	No	2048	68.2	84.6	89.2	80.1	88.8	91.6
ResNet50-GeM-CL	Yes	1024	72.4	86.6	90.4	88.7	93.9	95.4
ResNet50-GeM-GCL	Yes	1024	80.9	91.4	94.3	92.2	95.6	96.8
ResNet152-avg-CL	No	2048	51.3	73.0	80.1	73.5	86.4	89.9
ResNet152-avg-GCL	No	2048	64.0	83.6	89.2	78.9	89.0	91.9
ResNet152-avg-CL	Yes	1024	69.6	85.9	90.6	90.7	95.1	96.3
ResNet152-avg-GCL	Yes	2048	80.9	92.2	95.3	94.0	96.7	97.3
ResNet152-GeM-CL	No	2048	60.7	79.0	85.1	77.8	88.3	91.2
ResNet152-GeM-GCL	No	2048	68.0	84.9	89.8	81.5	90.3	92.8
ResNet152-GeM-CL	Yes	2048	76.2	89.9	93.4	91.1	95.3	96.4
ResNet152-GeM-GCL	Yes	2048	83.8	93.7	96.1	93.1	96.1	96.8
ResNeXt-avg-CL	No	2048	44.2	65.8	73.9	69.0	82.3	86.3
ResNeXt-avg-GCL	No	2048	57.9	76.1	82.6	77.7	86.9	89.7
ResNeXt-avg-CL	Yes	1024	69.6	85.4	89.8	88.9	94.1	95.6
ResNeXt-avg-GCL	Yes	1024	74.7	88.0	91.7	89.6	94.6	95.9
ResNeXt-GeM-CL	No	2048	50.2	70.8	78.8	66.1	78.5	82.7
ResNeXt-GeM-GCL	No	2048	58.6	76.2	81.8	78.7	87.1	90.1
ResNeXt-GeM-CL	Yes	1024	70.3	85.2	89.6	87.2	93.1	94.5
ResNeXt-GeM-GCL	Yes	1024	78.2	90.1	93.1	91.8	95.4	96.6

Table 8. Generalization results of the models trained on the MSLS dataset for the Pittsburgh250k and TokyoTM benchmarks.

V2 [33] and Extended CMU Seasons [33]. As we observed also with the GeM models, the Global Average Pooling

models achieve better performance when PCA whitening is applied, up to a 72.3% top-5 recall on the test set of MSLS.

E.2. Composition of training batches.

Effective composition of training batches is important for the performance of VPR methods, as witnessed by the fact that existing methods deploy very expensive pair mining techniques to select samples that effectively contributes to training. Although we do not use pair mining, we studied the impact on the retrieval performance by constructing batches with image pairs that have different degrees of similarity. We consider four strategies. Strategy A includes 50% positive $(\psi \in [0.5, 1])$, 25% soft-negative $(\psi \in (0, 0.5))$ and 25% hard-negative ($\psi = 0$) pairs in each batch. For Strategy B, the batches contain an uniform distribution of pairs with different similarity, namely 25% of pairs with $\psi \in [0.75, 1]$, 25% with $\psi \in [0.5, 0.75)$, 25% with $\psi \in (0, 0.5)$ and 25% with $\psi = 0$. For strategy C, we compose the batches with 33.3% of pairs with $\psi \in [0.5, 1]$, 33.3% with $\psi \in (0, 0.5)$ and 33.3% with $\psi = 0$. Finally, for strategy D we include 50% of pairs with $\psi \in [0.5, 1]$ and 50% with $\psi \in [0, 0.5)$. Histograms of the distributions of similarity in the batches are shown in Figure 10. The most important aspect of composing the training batches is to select an adequate number of soft negative pairs (see Table 10), i.e. at least 25% of the pairs have similarity $\psi \in (0, 0.5)$, as done for strategy A, B and C. For the main experiments, we used strategy A.

			N	ISLS-	Val	M	SLS-	Test	Pitt	sburg	h30k	Т	okyo2	4/7	Robot	Car Sea	sons V2	Extended	1 CMU S	Seasons
Method	PCA_u	Dim	R@1	R@5	R@10	R@1	R@5	R@10	R@1	R@5	R@10	R@1	R@5	R@10	0.25m/2°	0.5m/5°	5.0m/10°	0.25m/2°	0.5m/5°	5.0m/10°
VGG-avg-CL	No	512	28.8	47.0	53.9	16.9	30.5	36.4	28.9	53.7	64.8	10.5	24.1	35.6	1.0	6.4	34.4	0.9	3.0	22.7
VGG-avg-GCL	No	512	48.8	67.8	73.1	21.5	31.4	37.9	42.1	66.9	77.3	20.0	42.5	52.1	2.3	12.5	51.7	2.3	7.2	43.3
VGG-avg-CL	Yes	128	35.0	53.4	60.1	35.2	47.3	54.1	47.1	69.5	78.3	16.2	28.9	40.0	2.3	10.0	42.0	2.1	6.6	34.9
VGG-avg-GCL	Yes	256	54.5	72.6	78.2	32.9	49.0	56.5	56.2	76.7	83.9	28.6	45.7	54.9	3.6	15.3	57.1	3.7	11.2	52.5
ResNet50-avg-CL	No	2048	44.3	60.3	65.9	24.9	39.0	44.6	54.0	75.7	83.1	20.6	40.0	50.2	3.1	12.6	51.0	2.6	7.8	43.4
ResNet50-avg-GCL	No	2048	59.6	72.3	76.2	35.8	52.0	59.0	62.5	82.7	88.4	24.1	44.1	54.6	2.9	12.9	56.3	3.1	9.7	55.1
ResNet50-avg-CL	Yes	2048	58.8	71.4	75.8	33.1	46.5	53.3	65.8	82.6	88.2	48.6	63.2	70.5	5.9	22.8	62.7	4.7	13.8	50.8
ResNet50-avg-GCL	Yes	1024	69.5	81.2	85.5	44.2	57.8	63.4	73.3	87.1	91.2	52.1	68.9	72.7	5.9	23.1	69.6	5.4	16.2	66.5
ResNet152-avg-CL	No	2048	53.1	70.1	75.4	29.7	44.2	51.3	59.7	80.3	87.0	27.0	48.6	58.4	2.5	13.1	56.6	3.0	9.2	49.9
ResNet152-avg-GCL	No	2048	65.1	80.0	83.8	43.5	59.2	65.2	69.3	87.2	91.3	32.1	52.1	62.2	3.3	13.5	59.9	3.6	11.0	61.2
ResNet152-avg-CL	Yes	1024	63.0	77.7	81.5	37.7	51.6	56.9	68.8	85.9	90.4	49.8	67.3	74.3	5.4	22.2	64.8	4.8	14.3	59.9
ResNet152-avg-GCL	Yes	2048	75.8	87.4	89.7	52.7	68.1	74.2	77.9	90.4	93.5	64.4	77.8	83.2	6.2	23.9	70.0	5.7	17.0	66.5
ResNeXt-avg-CL	No	2048	58.9	75.1	79.9	34.5	50.1	57.7	51.3	73.6	81.9	24.8	47.3	56.8	2.7	10.9	61.0	2.0	6.1	40.0
ResNeXt-avg-GCL	No	2048	72.2	85.1	87.3	51.5	66.9	71.7	62.9	81.0	87.1	39.4	58.1	68.9	2.7	12.4	63.1	3.3	10.2	57.7
ResNeXt-avg-CL	Yes	1024	71.6	84.7	88.0	46.5	62.9	68.9	69.2	85.3	89.6	44.8	63.5	73.6	4.8	20.4	70.6	4.6	13.4	58.6
ResNeXt-avg-GCL	Yes	1024	79.3	89.2	90.3	57.8	72.3	77.1	74.8	88.2	91.8	53.0	76.2	80.6	2.7	10.9	61.0	5.6	16.6	70.7

Table 9. Ablation study: all the models are trained on the MSLS train set and deploy a global average pooling layer. When PCA whitening is applied we report the descriptor size that achieves the best results on the MSLS validation set.

F. Results on the TB-Places dataset

The dataset TB-Places was designed for place recognition in garden [18, 19]. It contains images taken by a rover robot in a garden at the University of Wageningen, the Netherlands, over three years. The dataset was collected for the TrimBot2020 project [40]. It includes drastic viewpoint variations, as well as illumination changes. The garden is a very challenging small environment with repetitive textures.

The dataset consists of three subsets, i.e. W16, with 41k images taken in 2016; W17, with 11k images taken in 2017; and W18, with 23k images taken in 2018. As in [19] we use the W17 subset to train the models. We design two experiments. For the first one we use W17 as map (11k images) and W18 as query (23k images). With this configuration we test the robustness of our models w.r.t. changes between the map and the query sets. For the second experiment, we divide W18 into query (17k images) and map (6k images) to test the generalization capabilities of our models in the case both map and query sets were not used for training. In Fig. 11, we show a sketch of the trajectory that the robot covered for the recording of the reference map (blue trajectory) and query (orange trajectory) images. The query images were taken from locations not covered by map images, thus including substantial viewpoint variations.

Experiments and results We trained our method on the TB-Places dataset and show the results in Fig. 12. We considered three backbones, namely ResNet18, ResNet34, and DenseNet161, which learn descriptors of size 512, 512 and 2208, respectively. We trained them with the binary Contrastive Loss function and with our Generalized Contrastive Loss function. Furthermore, we compare them with the NetVLAD off-the-shelf model. For these experiments we use only a Global Average Pooling.

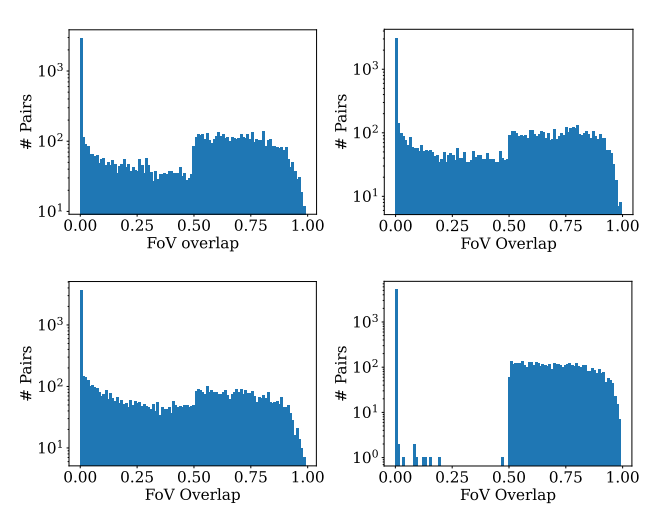


Figure 10. Similarity ground truth distribution for 10000 randomly selected pairs in the MSLS train set when using different batch composition strategies. The vertical axis is in log scale.

N/ 11	6.4		Strategy					
Model	Set	A	В	C	D			
VGG-GeM-GCL	Validation	77.8	78.8	78.2	73.4			
	Test	55.7	54.9	56	49.3			
ResNet50-GeM-GCL	Validation	78.9	76.5	75.7	75.4			
	Test	59.1	54.5	52.4	54.7			
ResNet152-GeM-GCL	Validation	82	80.4	78.6	78.5			
	Test	62.3	59.7	58.4	64.8			
ResNeXt-GeM-GCL	Validation	86.1	86.2	87.3	81.9			
	Test	70.8	70.7	72.4	64.8			

Table 10. Results (R@5) on the MSLS validation and test sets, using different training batch composition strategies.

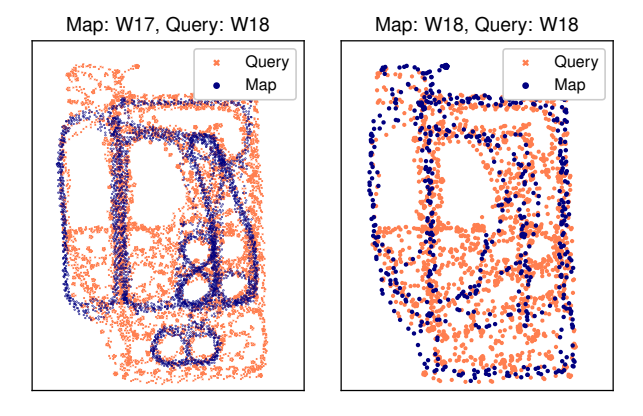


Figure 11. Configurations of the experiments on the TB-Places dataset. (a) W17 subset is the map set, and W18 is the query. (b) We divide W18 into map and query. For visualization purposes, the trajectories have been downsampled.

We report results of two experiments. For the first one, we used the training set W17 as map, and the W18 set as query. With this experiment we tested the strength of the descriptors against significant variations between the query and the map set. We show the results in Fig. 12a. For the second experiment, we divided the W18 set into map and query, to test the generalization capabilities when both map and query sets are unknown to the place recognition model (i.e. not seen during training). The results are displayed in Fig. 12b. For both experiments the models trained with GCL and the proposed similarity ground truth consistently achieve better recall than the ones trained with the binary Contrastive Loss, with the exception of the ResNet18.

G. Results on the 7Scenes dataset

The dataset A benchmark dataset for indoor camera localization [38]. It includes 26k training images and 17k test images, taken in seven environments. Each image has an associated ground truth 6DOF camera pose. Additionally, a 3D reconstruction of each scene is available. We use it to test our VPR models in indoor environments. For evaluation purposes, we define an image pair as a positive match if their annotated degree of similarity is higher than 50%. We use the training set as map, and the test set as query.

Experiments and results We report the results in Fig. 13. We used the ResNet18 and ResNet34 architectures as backbones with a Global Average Pooling layer and we compare them to NetVLAD off-the-shelf. We achieved generally higher Recall@K results for the models trained using the GCL function, for all scenes. The cases of the *stairs* (Fig. 13b), *chess* (Fig. 13f) and *office* (Fig. 13g) scenes are particularly interesting, since with the GCL descriptors we

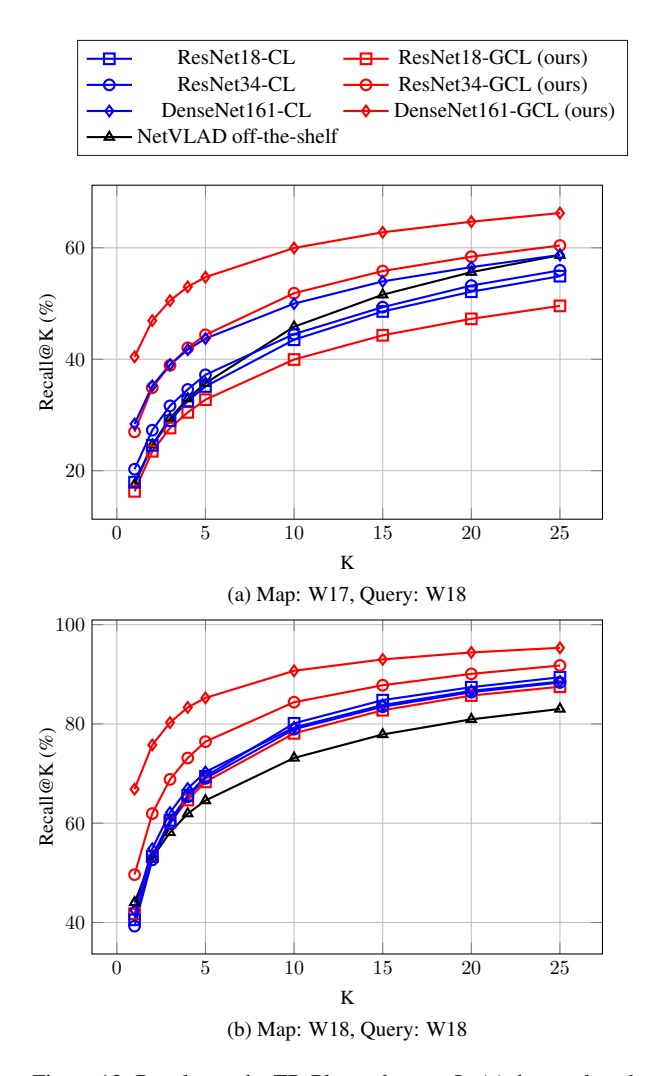


Figure 12. Results on the TB-Places dataset. In (a) the results when using W17 as map and W18 as query set. In (b) the top-k recall achieved when dividing W18 into map and query.

are able to retrieve positive matches for nearly all the query images, with a top-5 recall for ResNet34-GCL of 98.1%, 98.2% and 99.7%, respectively.

Furthermore, we report the average precision results in Table 11. The models trained with the GCL function achieved higher AP than their corresponding models trained with the binary CL function. We achieved an average AP equal to 0.89 using the ResNet34-GCL model.

H. GCL vs CL: Activation maps

In Fig. 14, we show the activation maps of the last convolutional layer of our models with a VGG16-GeM and a ResNet50-GeM backbone, both trained using the Contrastive Loss function (CL) and the proposed Generalized Contrastive Loss (GCL) function. We selected two example image pairs from the MSLS test set [48] (Kampala and

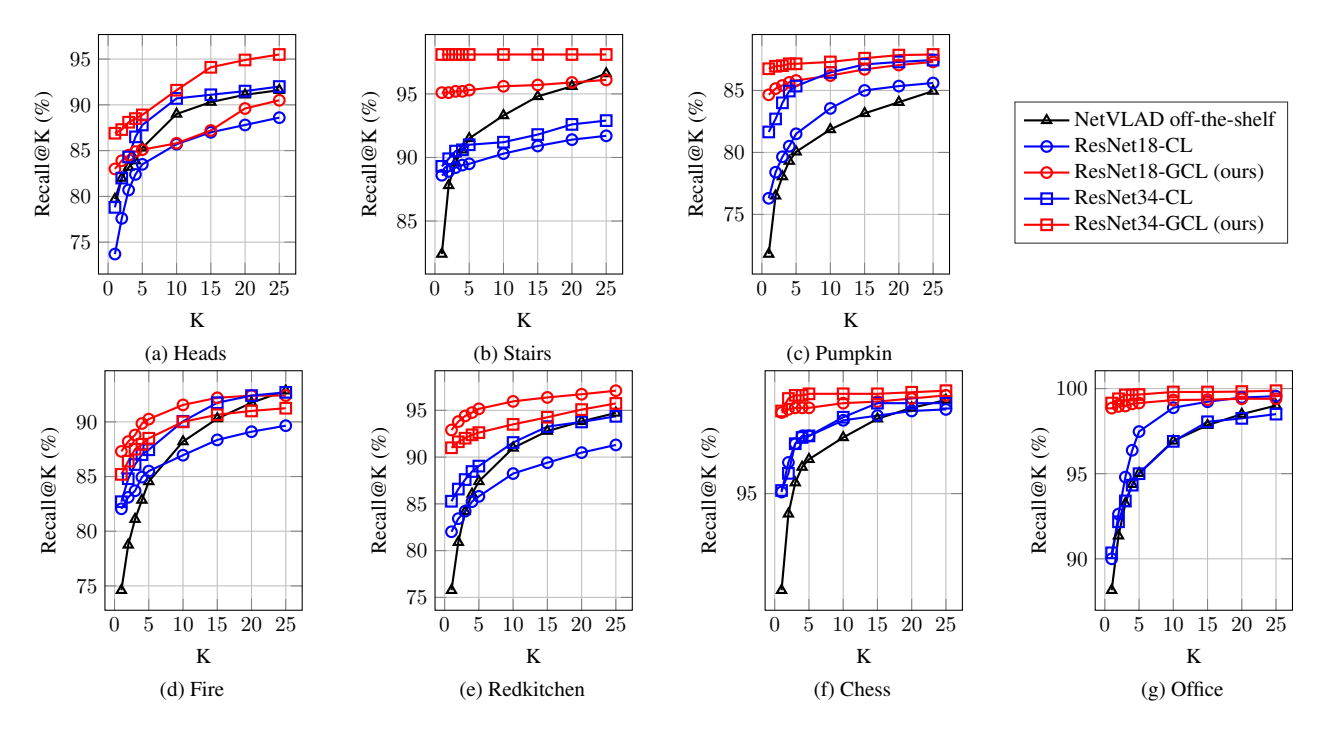


Figure 13. Recall@K results achieved on the 7 Scenes dataset. The results of the models trained with our Generalized Contrastive Loss are shown in red, while those of the models trained with the binary Contrastive Loss are shown in blue. The Recall@K achieved by NetVLAD off-the-shelf is plotted in black.

	NetVLAD	ResN	Net18	ResNet34			
Scene	off-the-shelf	CL	GCL	CL	GCL		
Heads	0.587	0.739	0.807	0.759	0.853		
Stairs	0.533	0.855	0.883	0.884	0.944		
Pumpkin	0.491	0.768	0.849	0.782	0.914		
Fire	0.539	0.786	0.811	0.796	0.803		
Redkitchen	0.439	0.790	0.876	0.782	0.902		
Chess	0.645	0.943	0.964	0.945	0.974		
Office	0.399	0.794	0.890	0.802	0.896		
Mean	0.519	0.811	0.868	0.821	0.898		

Table 11. Average Precision results obtained by the networks trained with the proposed Generalized Contrastive loss function on the 7Scenes dataset, compared with those achieved by the same network architectures trained using the binary Contrastive loss function and by the NetVLAD off-the-shelf model.

Stockholm), one from the Pittsburgh30k test set [2], and one from the Tokyo 24/7 dataset [43]. For all cases, we observed that the model trained with the GCL function produces higher activation for the common visual features of the images, and lower for the irrelevant parts (i.e. the road or the sky), in contrast to the model trained with the binary CL, which focuses less in the concerned areas of the pictures. In the example from Stockholm we can observe that our model does not respond to the cars (which vary from pic-

ture to picture), while it does respond strongly to the cranes (which are a longer-term cue). The example from Tokyo 24/7 is also particularly interesting: our model trained with the GCL function has high responses on the common parts of the images even under big changes of illumination. We observed that ResNet architectures tend to produce a peak of activation on the top left corner of the images. This does not seem to occur with the VGG architecture, so our intuition is that this artifact is due to the residual computation.

I. Gradient of the Generalized Contrastive Loss

Let us consider two input images x_i and x_j , their latent representations $\hat{f}(x_i)$ and $\hat{f}(x_j)$, and define $d(x_i, x_j)$ the Euclidean distance between the representations, such as:

$$d(x_i, x_j) = \left\| \hat{f}(x_i) - \hat{f}(x_j) \right\|_2$$

For simplicity of notation, hereinafter we refer to $d(x_i, x_j)$ as d.

I.1. Contrastive loss

The Contrastive Loss function is defined as:

$$\mathcal{L}_{CL} = \begin{cases} \frac{1}{2}d^2, & \text{if } y = 1\\ \frac{1}{2}\max(\tau - d, 0)^2, & \text{if } y = 0 \end{cases}$$

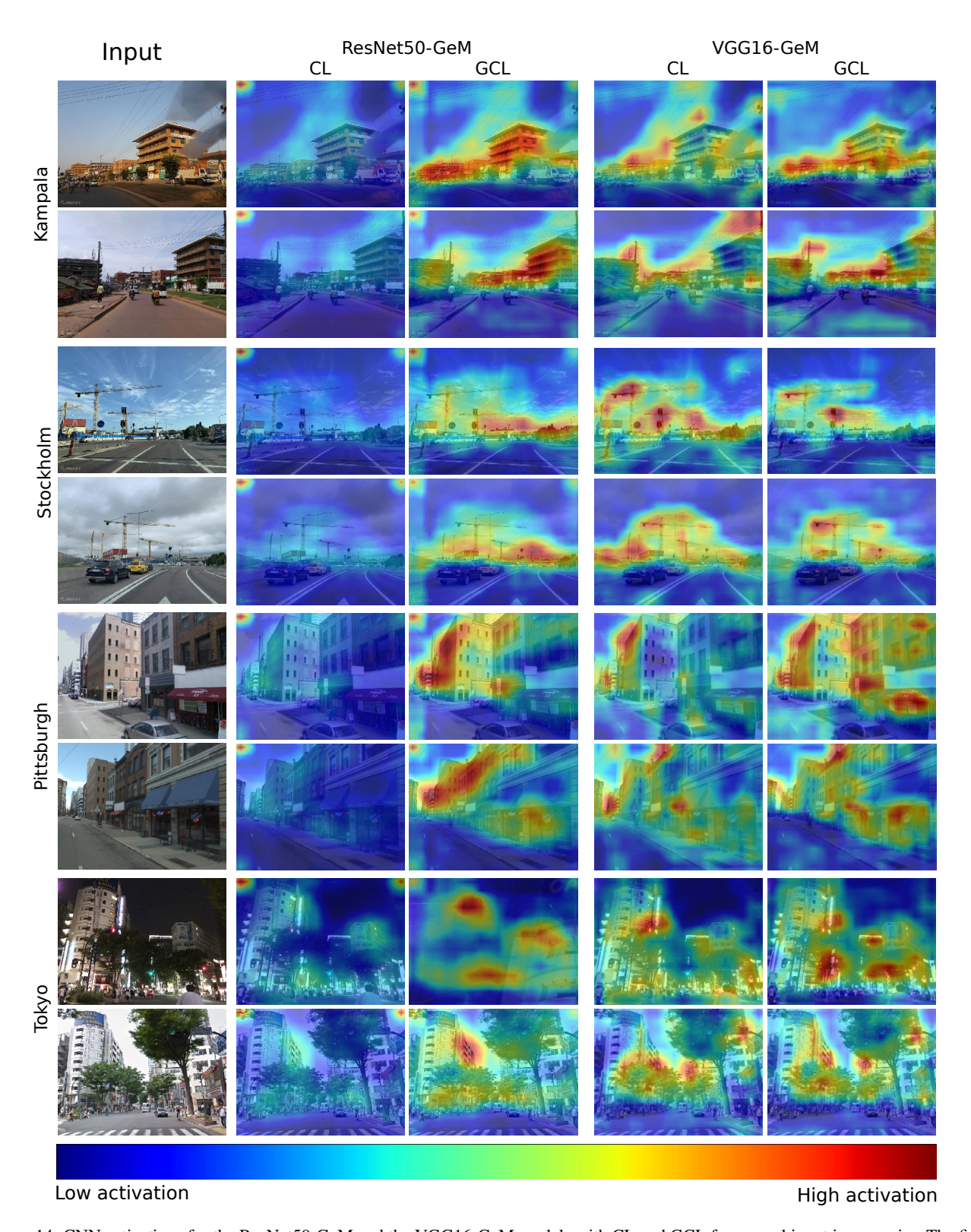


Figure 14. CNN activations for the ResNet50-GeM and the VGG16-GeM models with CL and GCL for several input image pairs. The first two pairs, corresponding to the first four columns, are part of the MSLS test set. The third and fourth belong to the Pittsburgh30k and Tokyo 24/7 test set, respectively. We show the activations for the last layer of the backbone overlapped with the input images.

where y corresponds to the binary ground truth label and τ corresponds to the margin.

In order to compute the gradient for this function, we consider three cases, depending on the ground truth label y and the value of the distance d.

Case 1)
$$y = 1$$

The loss function becomes:

$$\mathcal{L}_{CL} = \frac{1}{2}d^2$$

and its derivative with respect to d is:

$$\nabla \mathcal{L}_{CL} = \frac{\partial}{\partial d} \left(\mathcal{L}_{CL} \right) = \frac{\partial}{\partial d} \left(\frac{1}{2} d^2 \right) = d$$

Case 2) $y = 0, d < \tau$ The loss function becomes:

$$\mathcal{L}_{CL} = \frac{1}{2}(\tau - d)^2$$

and its derivative with respect to d is:

$$\nabla \mathcal{L}_{CL} = \frac{\partial}{\partial d} \left(\mathcal{L}_{CL} \right) = \frac{\partial}{\partial d} \left[\frac{1}{2} (\tau - d)^2 \right] = (\tau - d)(-1) = d - \tau$$

Case 3) $y = 0, d \ge \tau$

$$\mathcal{L}_{CL} = 0$$

and the gradient $\mathcal{L}_{CL}=0$ as well. Thus, case 2 and case 3, for y=0, can be grouped as:

$$\nabla \mathcal{L}_{CL} = \begin{cases} d - \tau, & \text{if } d < \tau \\ 0, & \text{if } d \ge \tau \end{cases}$$

and simplified as:

$$\nabla \mathcal{L}_{CL} = \min(d - \tau, 0)$$

Finally, the gradient of the Contrastive Loss function is:

$$\nabla \mathcal{L}_{CL} = \begin{cases} d, & \text{if } y = 1\\ \min(d - \tau, 0), & \text{if } y = 0 \end{cases}$$

I.2. Generalized Contrastive loss

We defined the Generalized Contrastive Loss function as:

$$\mathcal{L}_{GCL} = \psi_{i,j} \cdot \frac{1}{2} d^2 + (1 - \psi_{i,j}) \cdot \frac{1}{2} \max(\tau - d, 0)^2$$

where $\psi_{i,j}$ is the ground truth degree of similarity between the input images x_i and x_j , and its values are in the interval [0,1]. To compute the gradient of the GCL function we consider two cases, namely when 1) the distance d between the representations is lower than the margin τ and 2) the alternative case when d is larger than τ .

Case 1) $d < \tau$ The Generalized Contrastive loss function becomes:

$$\mathcal{L}_{GCL} = \psi_{i,j} \cdot \frac{1}{2}d^2 + (1 - \psi_{i,j}) \cdot \frac{1}{2}(\tau - d)^2$$

and its derivative with respect to d is:

$$\nabla \mathcal{L}_{GCL} = \frac{\partial}{\partial d} \left[\psi_{i,j} \cdot \frac{1}{2} d^2 + (1 - \psi_{i,j}) \cdot \frac{1}{2} (\tau - d)^2 \right] =$$

$$= \psi_{i,j} \cdot d + (1 - \psi_{i,j}) (\tau - d) (-1) =$$

$$= \psi_{i,j} \cdot d + d - \tau - \psi_{i,j} \cdot d + \psi_{i,j} \cdot \tau =$$

$$= d + \tau (\psi_{i,j} - 1)$$

Case 2) $d \geq \tau$

The Generalized Contrastive loss function becomes:

$$\mathcal{L}_{GCL} = \psi_{i,j} \cdot \frac{1}{2} d^2 + (1 - \psi_{i,j}) \cdot \frac{1}{2} (0)^2 = \psi_{i,j} \cdot \frac{1}{2} d^2$$

and its derivative with respect to d is:

$$\nabla \mathcal{L}_{GCL} = \frac{\partial}{\partial d} \mathcal{L}_{GCL} = \frac{\partial}{\partial d} \left[\psi_{i,j} \cdot \frac{1}{2} d^2 \right] = d \cdot \psi_{i,j}$$

Finally, the **gradient of the Generalized Contrastive Loss function** is:

$$\nabla \mathcal{L}_{GCL} = \begin{cases} d + \tau(\psi_{i,j} - 1), & \text{if } d < \tau \\ d \cdot \psi_{i,j}, & \text{if } d \ge \tau \end{cases}$$
 (5)